

AD-A087 245

STANFORD UNIV CA EDWARD L GINZTON LAB
LASER PHYSICS AND LASER TECHNIQUES.(U)
FEB 80 A E SIEGMAN, R L BYER

F/G 20/5

UNCLASSIFIED

GL-3093

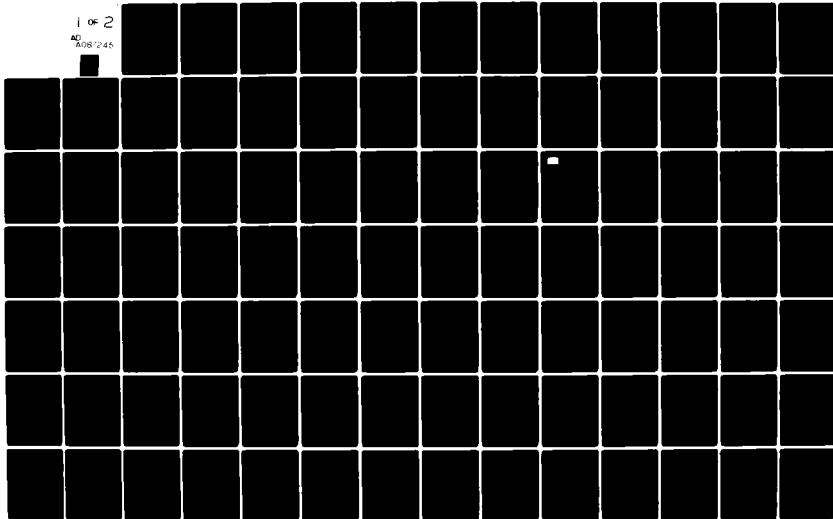
AFOSR-TR-80-0551

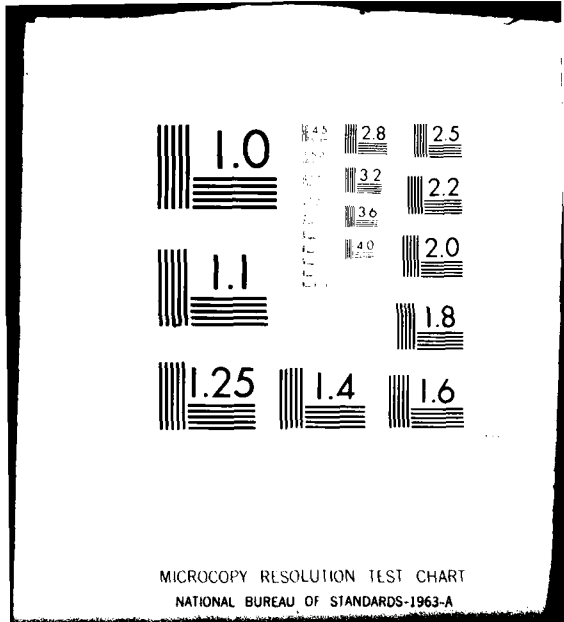
F49620-77-C-0092

NL

1 of 2

40
A087245





AEOSR-TR- 80-0551

LEVEL II

12

Edward L. Ginzton Laboratory
W. W. Hansen Laboratories of Physics
Stanford University
Stanford, California

ADA 087245

LASER PHYSICS AND LASER TECHNIQUES

Final Technical Report

for

Air Force Office of Scientific Research

Contract No. F49620-77-C-0092

for the period

1 January 1977 - 31 December 1979

RECEIVED
JUL 29 1980

Principal Investigators:

Professor A. E. Siegman
Professor R. L. Byer

G. L. Report No. 3093

February 1980

Approved for public release;
distribution unlimited.

DDC FILE COPY

33 7 28

UNCLASSIFIED

SECURITY CLASSIFICATION OF THIS PAGE (When Data Entered)

REPORT DOCUMENTATION PAGE		READ INSTRUCTIONS BEFORE COMPLETING FORM
1. REPORT NUMBER 18 AFOSR TR-80-0551	2. GOVT ACCESSION NO. AD-A087245	3. RECIPIENT'S CATALOG NUMBER
4. TITLE (and Subtitle) 6 LASER PHYSICS AND LASER TECHNIQUES	5. TYPE OF REPORT & PERIOD COVERED 9 Final Technical Report 1 JAN 1977 - 31 DEC 1979	
7. AUTHOR(s) Professor A.E. Siegman Professor R.L. Byer	6. PERFORMING ORGANIZATION REPORT NUMBER G.L. Report No. 3093	
9. PERFORMING ORGANIZATION NAME AND ADDRESS Edward L. Ginzton Laboratory Stanford University Stanford, California 94305	8. CONTRACT OR GRANT NUMBER(s) 15 F49620-77-C-0092	
11. CONTROLLING OFFICE NAME AND ADDRESS Air Force Office of Scientific Research Bolling AFB, Bldg. 410 Wash DC 20332	10. PROGRAM ELEMENT, PROJECT, TASK AREA & WORK UNIT NUMBERS 12 61102F 16 2301A1	
14. MONITORING AGENCY NAME & ADDRESS (if different from Controlling Office) 12 98 14 GL-309E	12. REPORT DATE 11 Feb 1980	
	13. NUMBER OF PAGES 96	
	15. SECURITY CLASS. (of this report) UNCLASSIFIED	
	15a. DECLASSIFICATION/DOWNGRADING SCHEDULE	
16. DISTRIBUTION STATEMENT (of this Report) Approved for public release; distribution unlimited.		
17. DISTRIBUTION STATEMENT (of the abstract entered in Block 20, if different from Report)		
18. SUPPLEMENTARY NOTES		
19. KEY WORDS (Continue on reverse side if necessary and identify by block number) Nonlinear Optics Bessel Transform Harmonic Generation Optically Pumped Laser Optical Parametric Oscillation Mercury Laser Hankel Transform Laser Frequency Stabilization		
20. ABSTRACT (Continue on reverse side if necessary and identify by block number) → A three-year program of research in laser physics and techniques has been carried out to help meet Air Force mid- and long-term requirements, as outlined in the AFSC Research Planning Guide. Development of an optically pumped atomic mercury laser was completed. Picosecond spectroscopy experiments led to measurements of ultrafast relaxation and diffusion times in solids. Work on efficient numerical methods for optical resonator calculations resulted in a Fast Hankel Transform for calculations in cylindrical		

UNCLASSIFIED

SECURITY CLASSIFICATION OF THIS PAGE(When Data Entered)

coordinates. Improvements to the FHT algorithm have been made and a two-stage algorithm developed.

An efficient procedure for analyzing nonlinear beam interactions has been developed; also several fundamental questions on aspects of laser resonators have been resolved. A diffraction-biased ring unstable resonator was invented, and an analysis of phase conjugate mirror resonators carried out. Studies of optically pumped lasers including mercury dimer as a potential laser mechanism were carried out. A number of two photon laser systems were investigated, and studies of four-wave mixing as a frequency conversion process completed. Improvements in the growth of lithium niobate crystals led to higher power tunable infrared and visible sources. Finally, stimulated rotational Raman scattering was demonstrated for efficient frequency conversion in the infrared.

UNCLASSIFIED

TABLE OF CONTENTS

	<u>Page</u>
I. INTRODUCTION	1
II. REVIEW OF ACCOMPLISHMENTS	2
A. Optically Pumped Atomic Mercury Laser	2
B. Picosecond Spectroscopy Experiments	3
C. Fast Transform Calculation Methods for Optical Beam and Resonator Calculations	4
D. Calculation Methods for Nonlinear Wave Interactions	6
E. Basic Laser Resonator Theory	7
F. Diffraction-Biased Ring Unstable Resonators	8
G. Phase Conjugate Mirror Resonators	9
H. Hg ₂ Optical Pumping Studies	9
I. Two Photon Laser Studies	11
J. Frequency Conversion via Four Wave Mixing	12
K. Optical Parametric Oscillator and Optical Parametric Amplifier Studies	13
L. Efficient Frequency Conversion via Stimulated Raman Scattering	15
M. Current Research	17
REFERENCES	18
III. PUBLICATIONS AND CONFERENCE PAPERS	21

AIR FORCE OFFICE OF SCIENTIFIC RESEARCH (AFSC)
NOTICE OF CONFIDENTIALITY
This technical report has been reviewed and is
approved for distribution under IAW AFR 190-12 (7b).
Distribution is unlimited.
AY D. BLOSE
Technical Information Officer

TABLE OF CONTENTS (cont'd)

	<u>Page</u>
IV. PROFESSIONAL PERSONNEL ASSOCIATED WITH THE RESEARCH EFFORT.	25
A. Ph.D. Graduates	25
B. Outside Visitors - Postdoctorates	27
V. OUTSIDE INTERACTIONS.	28
APPENDICES: Abstracts and/or Reprints.	29
I. Saturable Absorber Overlap of Iodine 127 with the Optically Pumped 546-nm Mercury Laser	30
II. Laser Induced Photoacoustic Grating Effects in Molecular Crystals.	32
III. Diffraction-Biased Unstable Ring Resonators with Possible Applications in Laser Gyroscopes	39
IV. Quasi Fast Hankel Transform	44
V. Orthogonality Properties of Optical Resonator Eigenmodes.	47
VI. Resonant Modes of Optical Cavities with Phase- Conjugate Mirrors	50

I. INTRODUCTION

This final report covers the three year contract period 1 January 1977 through December 31, 1979. During this time research work has been carried out by Professor A.E. Siegman in the areas of mercury lasers, picosecond spectroscopy, and optical beam and resonator calculations; and by Professor R.L. Byer in the areas of optically pumped lasers; two-photon laser systems, optical parametric amplifier oscillator studies, and stimulated rotational Raman scattering. During the past three year contract period important results have been obtained, including:

- A. Optically Pumped Atomic Mercury Laser
- B. Picosecond Spectroscopy Experiments
- C. Fast Transform Calculation Methods for Optical Beam and Resonator Calculations
- D. Calculation Methods for Nonlinear Wave Interactions
- E. Basic Laser Resonator Theory
- F. Diffraction-Biased Ring Unstable Resonators
- G. Phase Conjugate Mirror Resonators
- H. Hg₂ Optical Pumping Studies
- I. Two Photon Laser Studies
- J. Frequency Conversion via Four Wave Mixing
- K. Optical Parametric Oscillator and Optical Parametric Amplifier Studies
- L. Efficient Frequency Conversion via Stimulated Raman Scattering.
- M. Current Research.

Accession For	
NTIS	GRA&I
DDC	TAB
Unannounced Justification	
By _____	
Distribution/	
Availability Codes	
Dist	Available for special
A	

Details of these results are given below together with the resulting publications and the five Ph.D. theses which have been completed during this period.

II. REVIEW OF ACCOMPLISHMENTS

A. Optically Pumped Atomic Mercury Laser

During the early part of this program we were engaged in developing under AFOSR support a new optically pumped mercury laser oscillating at 5461 Å in the green. This laser oscillates in a laser tube containing a mixture of nitrogen and mercury, when pumped by a special high-brightness mercury discharge lamp. Because this laser involves no noisy plasma discharge in the laser tube itself, and because it oscillates at a convenient green wavelength, it is of particular interest as a possible laser gyro gain medium; as a visible wavelength standard; and possibly as a general purpose low-power green laser.

During the first year of the program reported here, the work on this project was brought to a successful conclusion and then terminated. A special diffusion-bypass low-pressure mercury arc lamp to meet the pumping needs of this laser with minimum mercury fill requirements, suitable for single-isotope operation, was invented, constructed, and operated very successfully for many hundreds of hours. Parametric studies of the laser itself, including measurements of gain and power output as functions of pressure, bore diameter and pumping intensity, were carried out.

Because this laser is of particular interest as a visible wavelength standard, measurements of saturated absorption in iodine using this laser formed one of the major goals of this program. These measurements were

carried out, and a strong, isolated saturated-absorption feature in $^{127}\text{I}_2$ was observed. The pressure shift of the laser transition against this iodine resonance was measured, and it was found possible to center the Hg laser transition exactly on the iodine resonance by varying the nitrogen pressure in the laser tube. These results laid a firm foundation for possible later absolute wavelength stabilization of this laser against a low-pressure iodine cell.

Work on this topic under AFOSR support was reported in detail in the following publications:

- Max Artusy and A. E. Siegman, "Saturable Absorber Overlap of Iodine 127 with the Optically Pumped 546 nm Mercury Laser," *Appl. Phys. Letters* 31, 333-334 (1 September 1977).
- Max Artusy, "Optically Pumped Mercury Laser for Absolute Frequency Stabilization," Ph.D. Dissertation, Department of Electrical Engineering, Stanford University, Stanford, California, 1977.

B. Picosecond Spectroscopy Experiments

Some very interesting measurements of ultrafast relaxation times in solids were completed during this program, using the novel transient laser-induced grating technique for picosecond spectroscopy developed in our group. The measurements demonstrated in particular a novel photo-acoustic pressure-induced amplitude grating effect in molecular crystals, of a type which does not appear to have ever been observed previously. This work was reported at the 1978 OSA Meeting and in a journal article, of which a reprint is attached as Appendix I of this report, as well as in a Ph.D. dissertation:

- J. R. Salcedo and A. E. Siegman, "Laser Induced Photoacoustic Grating Effects in Molecular Crystals," IEEE J. Quant. Electr. QE-15, 250-256 (April 1979).
- J. R. Salcedo, "The Picosecond Transient Grating Technique: Studies on Energy Transport and Photo-acoustic Effects," Ph.D. Dissertation, Stanford University, Stanford, California (February 1979).
- J. R. Salcedo and A. E. Siegman, "Amplitude Grating Effects Produced by Picosecond Laser Produced Acoustic Waves," (Paper THCl0, abstract only), J. Opt. Soc. Am. 68, 1412 (October 1978).
Paper presented at the 1978 Annual Meeting of OSA.

Work on this type of picosecond measurement using the transient grating approach is continuing in Professor Siegman's laboratory, and has been adopted by other groups elsewhere.

C. Fast Transform Calculation Methods for Optical Beam and Resonator Calculations

One of our primary research areas has been the development and verification of efficient and accurate numerical methods for handling optical beam and resonator calculations that are amenable to purely analytic treatment. This includes many situations of importance in high power and high energy lasers. One of our most important contributions has been a quasi Fast Hankel Transform technique for handling beam calculations in cylindrical coordinates (in contrast to Fast Fourier Transform techniques, which apply in rectangular coordinates).

In addition to the first publication of this transform algorithm, during the contract period substantial steps were accomplished in

completing and testing the novel Fast Hankel transform algorithm that we first invented, and in applying it to optical calculations, particularly to beam and resonator calculations. This new FHT algorithm, first published under AFOSR support in mid-1977, has since aroused wide interest and been used in several other AFOSR-supported industrial high-power laser programs.

Improvements to the original FHT algorithm under this program during the past year have included a simple "lower end correction" technique to compensate for the finite truncation of the transform integral at the lower end of the integration range; more accurate ways of handling the discrete Fast Fourier transform steps involved in the calculation; and better understanding of the choice of sampling intervals in the calculation. These improvements brought the accuracy of the transform close to the limits of single precision arithmetic on our machine (fractional error $\sim 10^{-6}$). In addition, a two-stage FHT algorithm requiring roughly twice the storage and computation time was developed which reduces the error of the algorithm itself, within its range of validity, to below $\sim 10^{-12}$ which is probably better than will ever be needed.

Publications that have appeared, or are in the final stages of preparation, covering the FHT algorithm include:

- A. E. Siegman, "Quasi Fast Hankel Transform," Optics Letters 1, 13-15 (July 1977).
- Shinan-Chur Sheng, "Studies of Laser Resonators and Beam Propagation Using Fast Transform Methods," Ph.D. Dissertation, Department of Applied Physics, Stanford University, Stanford, California (1980).

- A. E. Siegman and Shinan-Chur Sheng, "The Fast Hankel Transform Algorithm," manuscript in preparation (1980).

D. Calculation Methods for Nonlinear Wave Interactions

Another result of our program has been the development of an efficient procedure for analyzing important nonlinear interactions, such as harmonic generation and parametric or Raman amplification, including realistic considerations such as arbitrary beam profiles, diffraction and depletion effects, phase mismatch and walk-off, though not (for the minute) time-varying effects. An efficient procedure for analyzing such phenomena is important because these interactions provide an important way in which the energy of an efficient laser beam at one wavelength can be converted into useful and powerful radiation at other wavelengths, either longer or shorter, where an efficient laser system may not be available. One immediately important example is harmonic generation and parametric amplification with strong depletion, using an unstable resonator beam as the primary source, since this has already become an important practical technique for generating new coherent wavelengths.

We have therefore developed and made preliminary use of an efficient numerical method that accomplishes these objectives. To carry out the nonlinear interaction calculations we Fourier or Hankel transform the relevant nonlinear wave equation in its transverse coordinates, and obtain coupled differential equations of the form $dE_i/dz = F_i[E_j]$, where $E_i = E_i(s, z)$ is a spatially transformed wave at the i -th frequency ω_i and s is the transverse transform coordinate(s). Optical diffraction effects can be entirely transformed away in this transformation, so that

the function $F_1[E_1]$ contains only the nonlinear interaction of the wave E_1 with all other E_j components. Fast Fourier or Hankel transform methods are used to evaluate the derivative functions $F_1[E_1]$, and standard predictor-corrector ordinary differential equation (ODE) methods are used to step forward along z .

A preliminary account of this work was presented in 1977, and a full published report is now in press:

- A. E. Siegman and Shinan-Chur Sheng, "Optical Beam Calculations Using the Fast Hankel Transform," (Paper FD10, Abstract only), J. Opt. Soc. Am. 68, 1436 (October 1978). Paper presented at the 1978 Annual Meeting of the OSA.
- Shinan-Chur Sheng and A. E. Siegman, "Nonlinear-Optical Calculations Using Fast-Transform Methods: Second-Harmonic Generation with Depletion and Diffraction," to be published in Phys. Rev. A (1980).

E. Basic Laser Resonator Theory

Despite the now rather advanced state of laser theory, several very fundamental aspects of laser resonators have until recently remained unclear or uncertain. For example, because the fundamental propagation kernel in optical resonator theory is not a hermitian operator, the eigenmodes of optical resonators are not normal (i.e., orthogonal) modes, and the orthogonality properties of optical resonator modes have remained uncertain. All laser analyses to date have nonetheless obtained laser cavity equations of motion by assuming a hypothetical set of lossless and orthogonal cavity modes, despite the fact that real optical resonator modes have significant diffraction losses and are not orthogonal.

All of these fundamental questions have been essentially resolved under this program during the past year. The orthogonality properties of optical resonators have been found to be, in essence, that each eigenmode going in one direction in an optical cavity is orthogonal to all the other eigenmodes of an adjoint (biorthogonal) set of modes going in the opposite direction in the same cavity. In addition, a rigorous form of laser analysis has been developed which gives laser cavity equations of motion in terms of the real, lossy, nonorthogonal modes of the real laser cavity. This new analysis reduces to previous results in the appropriate limits, but is much better adapted to handle such topics as high-gain lasers with rapidly changing mode properties; lasers with external signal injection; and lasers with large spontaneous emission noise.

All of these results are reported in detail in the publications:

- A. E. Siegman, "Orthogonality Properties of Optical Resonator Eigenmodes," Optics Commun. 31, 369 (1979).
- A. E. Siegman, "Exact Cavity Equations for Lasers with Large Output Coupling," to be published in Appl. Phys. Letters 36 (1980).
- A. E. Siegman, "Cavity Equations for Laser Cavities with Large Output Coupling, Injected Signals, and Spontaneous Emission Noise," manuscript in preparation (1980).

F. Diffraction-Biased Ring Unstable Resonators

A novel type of diffraction-biased ring unstable resonator, with potential application to ring laser gyros, was invented and analyzed under this program. This result was published in:

- Shinan-Chur Sheng, "Diffraction-Biased Unstable Ring Resonators with Possible Applications in Laser Gyroscopes," IEEE J. Quant. Electr. QE-15, 922-926 (September 1979).

G. Phase Conjugate Mirror Resonators

One of the most interesting developments in optics in recent years has been the emergence of the phase conjugate mirror, using four-wave mixing, as a new fundamental optical component. During the past year, we have carried out a basic analysis of the resonator mode properties of optical cavities having a phase conjugate mirror at one end. These results are reported in detail in:

- Pierre A. Belanger, Amos Hardy, and A. E. Siegman, "Resonant Modes of Optical Cavities with Phase-Conjugate Mirrors," to be published in Appl. Optics 19 (1980).
- Pierre A. Belanger, Amos Hardy, and A. E. Siegman, "Resonant Modes of Optical Cavities with Phase Conjugate Mirrors: Higher-Order Modes," to be published in Appl. Optics 19 (1980).

H. Hg₂ Optical Pumping Studies

Research in optically pumped lasers occupied most of our effort in the first year of this program. The work built on our earlier success with the demonstration of the first electronic transition optically pumped laser in molecular I₂.¹ We followed the I₂ work by demonstrating an optically pumped Na₂ molecular laser.² Those early experiments did much to open the field of optically pumped lasers such that operation of a wide variety of lasers of this type has now been accomplished.

Under this program we extended our studies to Hg₂ because of its potential as an energy storage laser with tunable output. Our

theoretical studies led us to the concepts of energy storage in metastable states that are long lived because of radiation trapping. We also proposed to use an anti-Stokes process to extract the stored energy and suggested a specific process in atomic mercury.³ The energy storage method and the anti-Stoke extraction process were subjects of a patent application. However, the application is now dormant due to lack of Stanford interest.

Our experimental work in Hg_2 led almost immediately to the demonstration of a photodissociation laser in Hg which results from the dissociation of optically excited Hg_2 .⁴ This laser also represents a new class of devices and is an early form of recent photodissociation lasers based on alkali salts. Of particular interest, we observed laser action in atomic mercury on the strong $5461 \overset{\circ}{\text{A}}$ resonant transition.

Our main effort in these studies was to investigate molecular Hg_2 as a potential laser medium.⁵ Our measurements led to two principal results that affect the design of all high power gas laser sources. The first is that upper level absorption in molecular systems like Hg_2 leads to net loss for low cross-section laser transitions. The second is that three-body collision rates quench the storage levels so rapidly that energy storage in gases is not a useful approach for high energy density storage laser devices.

We specifically demonstrated these results for Hg_2 where we measured gain, loss, and collisional deactivation of the storage level. We also stated as a conclusion of our work, that low cross-sections for energy storage was not appropriate in gaseous systems. This point has now been conceded after three years of further research into the group six laser systems.

Our present understanding of high power or energy storage laser systems is further modified by optical damage problems. High energy storage laser systems must be designed not to exceed the damage limit of the resonator or external optical surfaces. For most laser systems this puts an effective limit on energy storage density and thus on the minimum useful cross-section required for efficient energy extraction. Interestingly, Nd:Glass is remarkably close to the optimum energy storage laser system based on these considerations alone.

I. Two Photon Laser Studies

To date, population inversion and subsequent stimulated emission via the two photon process has not been achieved. The interest in such a system is the potential for large energy storage and the potential for very large tunable output powers.

We investigated, in detail, a number of two photon laser systems which included atomic, molecular and solid state schemes. Our interests focused on atomic systems where the energy storage could be accomplished by optical pumping and the two photon laser action triggered by a high peak power infrared laser source. Atomic mercury, copper, calcium, strontium and barium were theoretically investigated. We also looked at two photon gain in nitrogen, oxygen and thallium. The result of the study showed that the required energy storage density was near 10^{18} atoms/cc for at least 1 μ sec duration. Our studies further showed that the two photon energy storage level must not be radiatively coupled to lower levels. The large energy storage density requirements led to a high pump laser energy level of greater than 100 mJ. At the time of the study the energy was greater than that available from our existing tunable laser sources.

As a second part of the program we investigated the triggering requirements to initiate two photon laser action, assuming that the inversion was available. This calculation, which is a major part of H. Komine's Ph.D. thesis,⁶ showed that efficient energy extraction from a two photon laser required a much greater initiation pulse energy than was previously thought. At the time of the program our existing tunable laser did not possess adequate energy for triggering a two photon laser system.

We have recently reconsidered the two photon laser source. The re-evaluation was brought about by our Raman studies and by the high pulse energy Nd:Glass tunable laser source now under construction. The laser technology and the understanding of the energy storage and laser trigger requirements make pursuit of a two photon laser a much more probable success now than four years ago. The benefits of high peak power tunable output are still present. An additional benefit is the possibility of stimulated anti-Stokes Raman up-conversion for both frequency shifting and energy gain toward the ultraviolet.

J. Frequency Conversion via Four Wave Mixing

We have recently completed theoretical and experimental studies of four wave mixing as a frequency conversion process. The initial concept was proposed in 1972 by Harris and Byer, but was not demonstrated until 1977.⁷ The early experiment showed that the 1.4 μm - 4.0 μm OPO tunable source could be frequency extended to cover the 4 μm - 18 μm spectral range by four wave mixing in H_2 gas.⁷

However, the early experiment was not in quantitative agreement with theory in that the observed mixing efficiency was a factor of 30 less than predicted.

In 1978 - 1979 we carefully studied the four wave mixing process in H_2 gas. During these measurements great care was taken to define the spatial and temporal aspects of the laser beams. The results were the major part of S. J. Brosnan's Ph.D. thesis which was completed in April 1979.⁸

Our concept of four wave mixing and a method to implement it led to a patent for the approach. Further, four wave mixing was shown to be an integral part of stimulated Raman scattering. Our increased understanding of the interaction of four wave mixing and stimulated Raman scattering led to the successful demonstration of $16 \mu m$ generation by four wave mixing, assisted stimulated rotational Raman scattering in para- H_2 gas using a CO_2 laser source.

K. Optical Parametric Oscillator and Optical Parametric Amplifier Studies

The need for higher power tunable infrared and visible sources led us to investigate improvements in the growth of $LiNbO_3$ by increasing the available crystal size. Our initial growth studies showed that large high quality $LiNbO_3$ crystals could be grown along the 01.4 direction.⁹ This growth direction is a few degrees off of the optimum phasematching angle for $1.06 \mu m$ pumped parametric oscillation.

We quickly demonstrated that 01.4 grown $LiNbO_3$ could be used for parametric oscillation over an extended $1.4 - 4.0 \mu m$ tuning range.¹⁰

Our work then proceeded toward the development of a computer controlled widely tunable, high energy source.

During the past three years we have achieved significant progress toward our goal of a fully automatic high resolution, reliable, tunable source.

We improved the LiNbO_3 crystal growth by continued research which led to a 01.3 growth axis and to crystals 20 mm in diameter by 6 cm in length. These crystals allow up to 0.1 J of tunable energy to be generated at 10 pps when pumped by a Nd:YAG source. We transferred the growth technology to a commercial firm which now supplies more than 50 crystals per year to customers around the world.

We developed a reliable Q-switched Nd:YAG pump source for the OPO measurements. A critical step in that work was the development of the unstable resonator Nd:YAG source¹¹ which is now the basis for the standard commercial Nd:YAG laser source.

We developed the first computer controlled tunable laser source with the capability to continuously scan over the widest wavelength range yet achieved in a single device. Recently our computer software and control capability has been transferred to commercial products. We demonstrated continuous tuning, data recording and data processing at 10 pps at 0.6 cm^{-1} linewidth over the 1.4 - 4.0 μm range. We used our tunable source capability in remote air pollution measurements¹² and in spectroscopic studies.¹³ Recently, we have successfully demonstrated continuous high resolution tuning at 0.08 cm^{-1} linewidth over a 20 cm^{-1} range and have taken long path absorption spectra of the atmosphere with the source. The OPO tuner has successfully operated for longer than one

year without crystal or component damage. Finally, we have demonstrated single axial mode operation of the OPO and have fully characterized crystal damage limitations, optimum OPO design and optimum pumping conditions.¹⁴

Our work on OPO tuners led to the consideration of optical parametric amplifiers as efficient power boosting devices with a wide tuning range. We successfully completed a detailed study of both a KD*P OPA and a LiNbO₃ OPA and for the first time verified the OPA theory by careful quantitative measurements.¹⁵ There is no doubt that OPA's will be used as wide bandwidth efficient power amplifiers in tunable laser systems.

Our work in this area was recently published in two papers in the Journal of Quantum Electronics.^{13,15} The work formed part of the Ph.D. thesis research of Dr. S. J. Brosnan and Dr. R. Baumgartner.

L. Efficient Frequency Conversion via Stimulated Raman Scattering

Our work in four wave mixing and our development of the high peak power Nd:YAG source led to the use of Stimulated Raman Scattering (SRS) to efficiently convert laser radiation to new frequencies.

During our Nd:YAG pumped Hg₂ and OPO studies we used SRS as a convenient means of efficiently generating new coherent wavelengths at both the Stokes and anti-Stokes shifted wavelengths. Our work led to a better understanding of the Raman process¹⁶ and to its general acceptance as a useful wavelength shifting method.¹⁷ SRS has now reached commercialization and is having significant impact because of the extended 1600 Å to 10 μm tuning range made available by SRS from a tunable dye laser source pumped via the unstable resonator Nd:YAG source.

Our early work in SRS led to the consideration of applying the technique in the infrared. A calculation showed that SRS could provide a useful method to efficiently convert 10 μm to 16 μm . The first paper proposing this concept was published by Byer in 1976.¹⁸ The proposal was met by general skepticism. However, we pursued the idea experimentally.

Our work in this area was partially funded by the Air Force and led to the concept of a multiple pass cell for enhancing the Raman gain. The paper describing the cell is to be published soon,¹⁹ and a patent is pending under the Air Force support.

Our persistent research effort led to the first successful stimulated rotational Raman scattering from para- H_2 at 10.6 μm .²⁰ We demonstrated 50 mJ of 16 μm output but more importantly a very high 40% photon conversion efficiency.²¹ Our results led to a careful theoretical evaluation of the optimum pump laser source and to a proposal for research in this area to AFOSR.²² Stimulated Rotational Raman Scattering is a conceptual breakthrough in infrared tunable sources in that it is not limited in peak or average power by the nonlinear element but only by the laser source. It is readily possible to design and demonstrate tunable IR output in the important 8 μm to 20 μm range at the Joules per pulse level at over 1 kHz repetition rate! A step in this direction was recently taken at Exxon²³ where 1.6 J at 16 μm was generated at 1 pps using an approach based on our research and our multiple pass cell concept.

The research in Stimulated Rotational Raman Scattering was the major part of W.R. Trutna's Ph.D. thesis. Dr. Trutna was a joint student under Professor A.E. Siegman and Professor R.L. Byer.

Our work in stimulated Raman scattering is continuing with the further development of theory and the application of SRS as a means of extending the tuning range of a Nd:Glass laser source. We are also planning experiments to demonstrate a Raman transfer laser and efficient picosecond pulse conversion via the stimulated Raman process.

M. Current Research

Our research in laser physics and laser techniques is currently generating new results in two areas. We have recently demonstrated Fourier transform limited single axial mode operation of an unstable Nd:YAG laser oscillator via injection locking. This work is part of the Ph.D. thesis of Y.K. Park and represents a technical achievement of some importance for both spectroscopic and military applications of the Nd:YAG source.

We are also pursuing the use of laser induced ionization as a new and very selective and sensitive detection and measurement tool. Research in this area will be the focus of our future research under this program.

We plan to continue to improve laser sources and tunable laser capability in support of our research effort. We also plan to continue to work toward obtaining patents whenever appropriate and to transfer our laser capability to the commercial community. Finally we recognize our responsibility to inform the AFOSR of any potential benefit to the Air Force resulting from our research.

REFERENCES

1. R.L. Byer, R.L. Herbst, H. Kildal and M.D. Levenson, "Optically Pumped Molecular Iodine," *Appl. Phys. Letts.* 20, p. 463 (1972).
2. M.A. Henesian, R.L. Herbst and R.L. Byer, "Optically Pumped Superfluorescent Na₂ Molecular Laser," *Journal Appl. Phys.* 47, p. 1515 (1976).
3. H. Komine and R.L. Byer, "Proposed Atomic Mercury Anti-Stokes Frequency Converter," *Appl. Phys. Letts.* 27, p. 300 (1975).
4. H. Komine and R.L. Byer, "Optically Pumped Atomic Mercury Photo-dissociation Laser," *Journal Appl. Phys.* 48, p. 2505 (1977).
5. H. Komine and R.L. Byer, "Optically Pumped Hg₂ Studies," *Journal Chem. Phys.* 67, p. 2536 (1977).
6. H. Komine, "Energy Storage and Two Photon Extraction from Metastable States," *Microwave Laboratory Report #2753*, November 1977, Ph.D. Thesis, Stanford University.
7. S.J. Brosnan, R.N. Fleming, R.L. Herbst and R.L. Byer, "Tunable Infrared Generation by Coherent Raman Mixing in H₂," *Appl. Phys. Letts.* 30, p. 330 (1977).
8. S.J. Brosnan, "Tunable Infrared Generation Using Parametric and Raman Processes," Ph.D. Thesis, Stanford University, Stanford, California, April 1979.
9. R.L. Byer, R.L. Herbst, R.S. Feigelson and W.L. Kway, "Growth and Application of (01.4) LiNbO₃," *Optics Commun.* 12, p. 427 (1974).
10. R.L. Byer, "Optical Parametric Oscillators," in Tunable Lasers and Applications, eds. A. Mooradian, T. Jasper, P. Stokseth, Springer-Verlag, 1976, p. 76-80.

11. R.L. Herbst, H. Komine and R.L. Byer, "A 200 mJ Unstable Resonator Nd:YAG Oscillator," *Optics Commun.* 21, p. 5 (1977).
12. R. Baumgartner and R.L. Byer, "Remote SO₂ Measurements at 4 μm With a Continuously Tunable Source," *Optics Letters* 2, p. 163 (1978).
13. N.I. Koroteev, M. Endemann and R.L. Byer, "Resolved Structure Within the Broad Band Vibrational Raman Line of Liquid H₂O from Polarization Coherent Anti-Stokes Raman Spectroscopy," *Phys. Rev. Letters* 43, p. 398 (1979).
14. S.J. Brosnan and R.L. Byer, "Optical Parametric Oscillator Threshold and Linewidth Studies," *Journal Quant. Electr.*, QE-15, p. 415 (1979).
15. R.A. Baumgartner and R.L. Byer, "Optical Parametric Amplification," *Journal Quant. Electr.* QE-15, p. 432 (1979).
16. W.R. Trutna, Y.K. Park and R.L. Byer, "The Dependence of Raman Gain on Pump Laser Bandwidth," *Journal Quant. Electr.* QE-15, p. 648 (1979).
17. R.L. Byer and R.L. Herbst, "The Unstable Resonator YAG," *Laser Focus*, July 1978, p. 48.
18. R.L. Byer, "A 16 μm Source for Laser Isotope Enrichment," *IEEE Journal Quant. Electr. Correspondence*, 732-733 (November 1976).
19. W.R. Trutna and R.L. Byer, "A Multiple Pass Raman Gain Cell," to be published in *Applied Optics*, February 1980.
20. R.L. Byer and W.R. Trutna, "16 μm Generation by CO₂ Pumped Rotational Scattering in H₂," presented at the 10th International Quantum Electronics Conference held in Atlanta, Georgia, June 1978 and published in the *Journal of the Opt. Soc. of Am.* 68, p. 1622 (1978).

21. R.L. Byer and W.R. Trutna, "16 μm Generation by CO_2 Pumped Rotational Raman Scattering in H_2 ," Optics Letters, 3, p. 144 (1978).
22. R.L. Byer, "Stimulated Rotational Raman Scattering in the Infrared," Proposal submitted to AFOSR, April 1979.
23. P. Rabinowitz, A. Stein, R. Brickman and A. Kaldor, "Efficient Tunable H_2 Raman Laser," Appl Phys. Letters 35, p. 739 (1979).

III. PUBLICATIONS AND CONFERENCE PAPERS

1. A. E. Siegman, "Quasi Fast Hankel Transform", Optics Letters 1, 13-15 (July 1977).
2. Max Artusy and A. E. Siegman, "Saturable Absorber Overlap of Iodine 127 with the Optically Pumped 546 nm Mercury Laser", Appl. Phys. Letters 31, 333-334 (1 September 1977).
3. Max Artusy, "Optically Pumped Mercury Laser for Absolute Frequency Stabilization", Ph.D. Dissertation, Department of Electrical Engineering, Stanford University, Stanford, California, 1977.
4. A. E. Siegman, Shinan-Chur Sheng, and Amos A. Hardy, "Nonlinear Optical Beam Calculations Using Transform Methods", J. Opt. Soc. Am. 67, 1396 (October 1977). Paper WG16 presented at the Annual Meeting of the Optical Society of America, Toronto, October 1977.
5. Hiroshi Komine, "Energy Storage and Two-Photon Extraction from Metastable States", Ph.D. Dissertation, Department of Applied Physics, Stanford University, Stanford, California, 1977.
6. S. J. Brosnan, R. N. Fleming, R. L. Herbst and R. L. Byer, "Tunable Infrared Generation by Coherent Raman Mixing in H₂", Appl. Phys. Letters 30, 330 (April 1977).
7. R. L. Byer and R. L. Herbst, "Parametric Oscillation and Mixing", in Nonlinear Infrared Generation, Y. R. Shen, ed., (New York: Springer-Verlag, 1977), Vol. 16.
8. H. Komine and R. L. Byer, "Optically Pumped Atomic Mercury Photo-dissociation Laser", J. Appl. Phys. 48, 2505 (1977).
9. H. Komine and R. L. Byer, "Optically Pumped Hg₂ Studies", J. Chem. Phys. 67 (September 1977).

10. R. L. Byer, "Parametric Oscillators and Nonlinear Materials", in Nonlinear Optics, Proceedings of the 16th Scottish Universities Summer School in Physics, Philip G. Harper and Brian S. Wherrett, eds., (London: Academic Press, 1977), p. 47.
11. A. E. Siegman and Shinan-Chur Sheng, "Optical Beam Calculations Using the Fast Hankel Transform", (Paper FD10, abstract only), J. Opt. Soc. Am. 68, 1436 (October 1978). Paper presented at the 1978 Annual Meeting of the O.S.A.
12. A. E. Siegman and Shinan-Chur Sheng, "The Fast Hankel Transform Algorithm". To be submitted for publication.
13. A. E. Siegman, Shinan-Chur Sheng, and Amos A. Hardy, "Nonlinear Optical Beam Calculations using Transform Methods", J. Opt. Soc. Am. 67, 1396 (October 1977). Paper WG16 presented at the Annual Meeting of the Optical Society of America, Toronto, Canada, October 1977.
14. Shinan-Chur Sheng, "Diffraction-Biased Unstable Ring Resonators with Possible Applications in Laser Gyroscopes", IEEE J. Quant. Electr. QE-15, 922-926 (September 1979).
15. J. R. Salcedo and A. E. Siegman, "Amplitude Grating Effects Produced by Picosecond Laser Produced Acoustic Waves", (Paper THC10, abstract only), J. Opt. Soc. Am. 68, 1412 (October 1978). Paper presented at the 1978 Annual Meeting of O.S.A.
16. J. R. Salcedo and A. E. Siegman, "Laser Induced Photoacoustic Grating Effects in Molecular Crystals", IEEE J. Quant. Electr. QE-15, 250-256 (April 1979).
17. J. R. Salcedo, "The Picosecond Transient Grating Technique: Studies on Energy Transport and Photo-acoustic Effects", Ph.D. Dissertation, Stanford University, Stanford, California (February 1979).

18. S. J. Brosnan and R. L. Byer, "Optical Parametric Oscillator Threshold and Linewidth Studies", invited paper, J. Quant. Electr. QE-15, no. 6, 415-431 (June 1979).
19. B. A. Baumgartner and R. L. Byer, "Optical Parametric Amplification", J. Quant. Electr. QE-15, no. 6, 432-444 (June 1979).
20. R. L. Baumgartner, "Optical Parametric Amplification and Applications to Remote Air Pollution Monitoring", Ph.D. Dissertation, Stanford University, Stanford, California (September 1978).
21. S. J. Brosnan, "Tunable Infrared Generation by Raman and Parametric Processes", Ph.D. Dissertation, Stanford University, Stanford, California (April 1979).
22. W. R. Trutna, Y. K. Park and R. L. Byer, "Dependence of Raman Gain on Pump Laser Bandwidth", J. Quant. Electr. QE-15, no. 7, 648-655 (July 1979).
23. W. R. Trutna, Y. K. Park and R. L. Byer, "The Bandwidth Independence of Stimulated Raman Scattering", presented at the OSA Meeting, October 1978, San Francisco, California.
24. R. L. Byer and W. R. Trutna, "16 μm Generation by CO_2 Pumped Rotational Raman Scattering in H_2 ", presented as a post-deadline paper at the International Quant. Electr. Conference, Atlanta, Georgia, June 1978; published in J. Opt. Soc. Am. 68, 1622 (1978).
25. R. L. Byer and W. R. Trutna, "16 μm Generation by CO_2 Pumped Rotational Raman Scattering in H_2 ", Optics Letters 3, 144 (1978).
26. R. L. Byer, "16 μm Generation via Stimulated Rotational Raman Scattering at 10 μm ", Invited paper, Optical Society of America Meeting October 1978, San Francisco, California.
27. S. J. Brosnan and R. L. Byer, "Infrared Generation via Four-Wave Mixing in H_2 Gas," to be published (1980).

28. W. R. Trutna and R. L. Byer, "A Multipass Cell and Application to Raman Scattering," *Appl. Optics* 19(2), 301 (1980).
- * 29. Shinan-Chur Sheng and A. E. Siegman, "Nonlinear-Optical Calculations Using Fast-Transform Methods: Second Harmonic Generation with Depletion and Diffraction," to be published in *Phys. Rev. A* (1980).
30. A. E. Siegman, "Orthogonality Properties of Optical Resonator Eigenmodes," *Optics Commun.* 31, 369 (1979).
- * 31. A. E. Siegman, "Exact Cavity Equations for Lasers with Large Output Coupling," to be published in *Appl. Phys. Letters* 36 (1980).
32. Pierre A. Belanger, Amos Hardy, and A. E. Siegman, "Resonant Modes of Optical Cavities with Phase-Conjugate Mirrors," to be published in *Appl. Optics* 19 (1980).
- * 33. Pierre A. Belanger, Amos Hardy, and A. E. Siegman, "Resonant Modes of Optical Cavities with Phase Conjugate Mirrors: Higher-Order Modes," to be published in *Appl. Optics* 19 (1980).
34. A. E. Siegman, "Cavity Equations for Laser Cavities with Large Output Coupling, Injected Signals, and Spontaneous Emission Noise," manuscript in preparation (1980).
- * 35. Shinan-Chur Sheng, "Studies of Laser Resonators and Beam Propagation Using Fast Transform Methods," Ph.D. Dissertation, Department of Applied Physics, Stanford University, Stanford, California (1980).
- * 36. A. E. Siegman and Shinan-Chur Sheng, "The Fast Hankel Transform Algorithm," manuscript in preparation (1980).
37. G. Giuliani, Y. K. Park, and R. L. Byer, "Stable Single Axial Mode Operation of an Unstable Resonator Nd:YAG by Injection Locking," to be published in *Optics Letters* (March 1980).

* To be provided upon publication.

IV. PROFESSIONAL PERSONNEL ASSOCIATED WITH THE RESEARCH EFFORT

A. Ph.D. Graduates

Dr. Max Artusy received the Ph.D. degree in Electrical Engineering under Professor Siegman (entirely under AFOSR support) in 1977, with a dissertation entitled, "Optically Pumped Mercury Laser for Absolute Frequency Stabilization". Dr. Artusy is now an Assistant Professor of Electrical Engineering at Georgia Institute of Technology.

Dr. Neil C. Holmes received the Ph.D. degree in Electrical Engineering under Professor Siegman (primarily under AFOSR support) in 1977, with a dissertation entitled, "The Optically Pumped Mercury Vapor Laser". Dr. Holmes is now a member of the technical staff at Lawrence Livermore Laboratory (DOE).

Dr. Jose Ribera Salcedo received the Ph.D. degree in Electrical Engineering under Professor Siegman (substantially under AFOSR support) with a dissertation entitled, "The Picosecond Transient Grating Technique: Studies on Energy Transport and Photoacoustic Effects". Dr. Salcedo has been an IBM Postdoctoral Fellow at Stanford University for the past year, and is now returning to Portugal.

Dr. Shinan-Chur Sheng will receive the Ph.D. degree in Applied Physics under Professor Siegman (entirely under AFOSR support) in early 1980, with a dissertation entitled, "Studies of Laser Resonators and Beam Propagation Methods Using Fast Transform Methods". Dr. Sheng has taken employment with Spectra-Physics, a leading laser firm.

Dr. W. R. Trutna, Jr. received his Ph.D. in Electrical Engineering under Professors R. L. Byer and A. E. Siegman (partially under AFOSR support) in 1979, with a dissertation entitled, "Generation of 16 Micron Radiation

Using Stimulated Rotational Raman Scattering in Hydrogen". Dr. Trutna has been a Post-doctoral Fellow at the Max Planck Research Institute, Garching, Germany, and will shortly be taking employment in a United States industrial firm.

Dr. H. Komine received his Ph.D. in November 1977 under Professor R. L. Byer in Applied Physics (substantially under AFOSR support). His thesis was entitled, "Energy Storage and Two Photon Extraction from Metastable States". He is now employed by Northrup Research Laboratories, California.

Dr. Richard Baumgartner received his Ph.D. in Electrical Engineering under Professor Byer in July 1978, with a dissertation entitled, "Optical Parametric Amplification". His work was partially supported by AFOSR. Dr. Baumgartner is now employed by Hewlett-Packard, Palo Alto Research Center, Palo Alto, California.

Dr. Stephen Brosnan received his Ph.D. in Applied Physics under Professor Byer (entirely supported by AFOSR) in June 1979. His dissertation was entitled, "Tunable Infrared Generation Using Parametric and Raman Processes". He is now employed by Quanta Ray Inc., Mountain View, California.

Mr. David C. Wolfe will receive his Ph.D. in Applied Physics under Professor Byer early in 1980 (substantially supported by AFOSR). His dissertation is, "Model Studies for the Application of Optical Tomography to Air Pollution Measurements".

Mr. Y. K. Park will receive his Ph.D. in Applied Physics under Professor Byer in early 1980 (entirely under AFOSR support). His dissertation concerns Single Axial Mode Operation of the Nd:YAG Laser by Injection Locking.

B. Outside Visitors - Postdoctorates

Outside visitors participating actively in the research for visiting periods of 6 months or longer (at no direct salary cost to the contract) included:

- Dr. Amos Hardy, Weizmann Fellow, from Weizmann Institute, Israel.
- Prof. Pierre Belanger, on sabbatical from Laval University, Quebec.
- Dr. Wolfram Schmid, on fellowship from the Max Planck Institute, Garching, Germany.
- Ms. Paola Ristori, University of Rome.
- Dr. H. Ito, Tohoku University, Sendai, Japan.
- Dr. Giampero Giuliani, University of Rome.
- Dr. Josef Unternahrer, Swiss Institute of Nuclear Research, Zurich, Switzerland.
- Dr. Nikolai Koroteev, Moscow State University, Moscow, USSR.

V. OUTSIDE INTERACTIONS

Numerous visitors from industrial and U.S. government laboratories and from foreign institutions visited this laboratory to interact with the faculty members and students during the period of this contract.

Professor Siegman has served as a member of the Air Force Scientific Advisory Board since 1974, including its Electro-Optics Panel, Panel on Basic Research, and various ad hoc committees. He has also been a regular consultant to United Technologies/Pratt and Whitney Aircraft, GTE Sylvania Electro-Optics Organization, and the Lawrence Livermore Laboratories (DOE).

He presented an invited paper on "Laser-Induced Grating Spectroscopy" at the Conference on Dynamical Processes in Solids, Madison, Wisconsin, in June 1979. An invited presentation on the same topic for the International Symposium on Ultrafast Phenomena in Spectroscopy, Tallin, Estonia, in October 1978 was scheduled but not presented. He earlier taught a "Short Course on Unstable Resonators" at the Optical Society of America annual meeting in San Francisco, October 1978.

Professor Byer has served the United States Government as a member of an Army Advisory Board to review research in Army laboratories. He has also served on the Lawrence Berkeley Laboratory Advisory Board and Review Committee. He is a consultant to Westinghouse, Bethlehem Steel Corporation, Allied Chemical, SRI International, and Quanta Ray Inc.

During this program Professor Byer has presented numerous invited papers. He has taught a laser course at George Washington University and a special course on nonlinear optics at the Optical Society of America Annual Meeting in San Francisco, October 1978.

APPENDICES I TO VI

Saturable absorber overlap of iodine 127 with the optically pumped 546-nm mercury laser^{a)}

Max Artusy and A. E. Siegman

Edward L. Ginzton Laboratory, Department of Electrical Engineering, Stanford University, Stanford, California 94305

(Received 23 May 1977; accepted for publication 23 June 1977)

A single isolated saturated-absorption feature in $^{127}\text{I}_2$ using the optically pumped 546.1-nm Hg laser has been observed with low (~ 6 MHz) resolution. The $^3\text{S}_1 \rightarrow ^3\text{P}_2$ Hg laser transition can be centered exactly on this feature by varying the N_2 buffer gas pressure using the measured pressure tuning rate of -9.4 MHz/Torr. This may provide an attractive laser system for absolute wavelength stabilization.

PACS numbers: 42.65.Gv, 32.70.Jz, 42.55.Hq

The optically pumped 546.1-nm mercury laser^{1,2} is potentially very attractive for frequency stabilization. The absence of any active discharge in the all-fused-quartz single-isotope gain cell should imply a nearly ideal long-lived laser medium especially suitable for high-stability applications, with minimum disturbance from gas cleanup, discharge instabilities, and cataphoresis. Laser oscillation is obtained by pumping the continuously flowing or sealed-off² Hg- N_2 laser tube with specially constructed low-pressure Hg lamps in a conventional double-ellipse pump cavity. A simplified energy-level diagram of the laser system is shown in Fig. 1. The 253.7-nm Hg resonance line populates the $^3\text{P}_1$ level of mercury, which is quenched to $^3\text{P}_0$ with the aid of ~ 30 Torr of N_2 . The less-intense mercury 404.7-nm line then pumps from $^3\text{P}_0$ to the Hg $^3\text{S}_1$ level, from which laser actions occur down to the $^3\text{P}_2$ level on the mercury green line at 546.1 nm. The nitrogen also quenches the $^3\text{P}_2$ lower laser level, without totally quenching the other excited mercury levels involved in the laser action.

Intense non-self-reversed pump lamps capable of operating with very small quantities of single isotope mercury have been developed for pumping this laser.

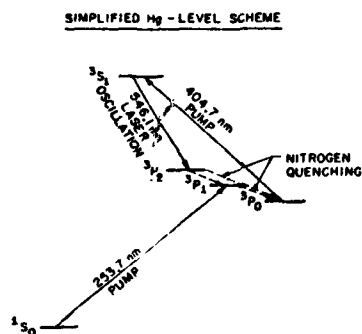


FIG. 1. Energy-level scheme of the optically pumped Hg- N_2 laser.

^{a)} Research was supported by the Air Force Office of Scientific Research. Thanks are due to Neil Holmes who has carried out other aspects of the Hg laser development and on whose apparatus some of these data were taken.

As with other metal-vapor-rare-gas discharges, cataphoresis is a problem of primary importance.³ To overcome this difficulty, we use the diffusion-bypass lamp design shown in Fig. 2. A 2-A dc discharge in the temperature-controlled capillary bore of this lamp cataphoretically pumps mercury from a cold reservoir near the anode to the cathode at a rapid rate. The parallel large-bore discharge-free tube then provides a diffusion return path through which the mercury can continuously diffuse back to the anode. Nickel baffles suppress the discharge in the return path while allowing free diffusion of the mercury. The vapor pressure within the lamp is varied by heating the recirculating deionized water and thus controlling the capillary bore temperature. All other parts of the lamp are kept warmer than the $\sim 50^\circ\text{C}$ water temperature to prevent mercury condensation elsewhere in the lamp. It has been found experimentally that the ion-laser-type tungsten dispenser cathodes do not absorb or getter the mercury.⁴ Typical lamp fill is 15 mg of ^{202}Hg and 500 μ of research-grade argon. Operating lifetime of a carefully prepared lamp appears to be at least several hundred hours without signs of deterioration.

Preliminary inverse Lamp-dip experiments using the mercury laser with an $^{127}\text{I}_2$ saturable absorption cell have been performed. A iodine cell was placed within the 1.25-m-long cavity of a piezotuned flowing-gas mercury laser. The Hg- N_2 laser itself has a pressure-broadening coefficient of ~ 20 MHz/Torr,⁴ and thus presumably operates in the transition region between fully homogeneously and inhomogeneously

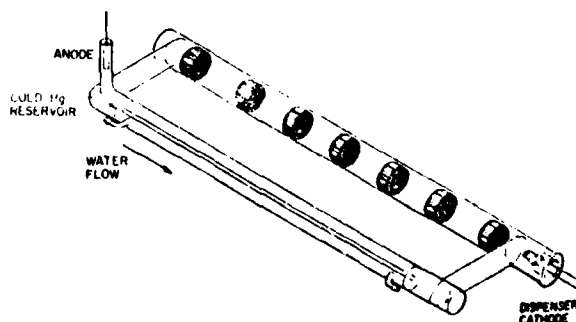


FIG. 2. Diffusion-bypass low-pressure Ar-Hg lamp developed for pumping the Hg- N_2 laser.

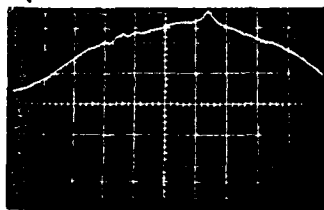


FIG. 3. Saturated absorption feature due to $^{127}\text{I}_2$ in a $^{202}\text{Hg}-\text{N}_2$ laser at ~ 24 Torr of N_2 .

broadened limits. In agreement with this, no laser Lamp dip has been observed, although multiple axial modes will oscillate simultaneously. Single axial mode operation was obtained by the pragmatic approach of reducing the pumping level to only slightly above threshold, giving a 120-MHz free-tuning range for the laser at fixed gas pressure. Within the available pressure and piezoelectric tuning range of this laser, only one inverted Lamb dip was observed, with a typical appearance as shown in Fig. 3. This single feature has a FWHM of ~ 6 MHz, approximately comparable to I_2 plus He-Ne systems previously investigated.⁵

One of the attractive features of this system is the readily observed pressure shift of the laser gain profile produced by the N_2 buffer gas. The Hg laser can be operated over a N_2 pressure range from at least 11 to 40 Torr. The pressure shift of the laser transition over the central portion of this range has been determined by observing the relative position of the I_2 inverted Lamb dip within the center of the laser's piezotuning range for various fixed gas pressures. The results of these measurements, as summarized in Fig. 4, show a pronounced red shift of -9.4 MHz/Torr. By adjusting the nitrogen pressure to approximately 25 Torr (which

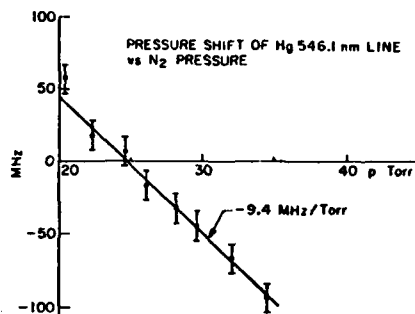


FIG. 4. Frequency shift of the Hg 546.1-nm laser transition relative to the $^{127}\text{I}_2$ saturated-absorption peak as a function of N_2 pressure in the Hg- N_2 laser tube.

is not too far from the optimum value for laser operation), the laser gain profile can be centered exactly below the inverted Lamb dip. This can minimize the necessity for third-derivative locking schemes to suppress slope offset problems encountered with the He-Ne and other lasers.⁵

Note added in proof. The iodine transition responsible for the saturated absorption feature has tentatively been identified as the $R(122)$ line of the $v''=2$ to $v'=34$ band.

¹N. Djeu and D. Burnham, *Appl. Phys. Lett.* 25, 350 (1974).

²Max Artusy, Neil Holmes, and A.E. Siegman, *Appl. Phys. Lett.* 28, 133 (1976).

³K.G. Hernqvist, *Appl. Phys. Lett.* 16, 1 (1970).

⁴Neil C. Holmes (private communication).

⁵W.G. Schweitzer, Jr., E.G. Kessler, Jr., R.D. Deslattes, H.P. Layer, and J.R. Whetstone, *Appl. Opt.* 12, 2927 (1973).

Laser Induced Photoacoustic Grating Effects in Molecular Crystals

JOSÉ R. SALCEDO AND ANTHONY E. SIEGMAN, FELLOW, IEEE

Abstract—A transient grating of singlet electronic excited states is produced in a pentacene-doped p-terphenyl molecular crystal by optical absorption from two crossed time-coincident picosecond excitation pulses at 532 nm. The diffraction properties of this volume grating are probed by a weak, variably delayed, Bragg-matched picosecond probe pulse. At high excitation intensities, a strong oscillatory behavior in the time-dependent scattering efficiency is observed superimposed on the exponential decay pattern of the excited-state grating. We attribute the oscillatory behavior to a thermal grating which induces coherent microwave acoustic phonons. These in turn modulate, at the sound frequency, the optical absorption properties of the pentacene molecules in the excited state. An acoustically induced *amplitude* grating effect is thus obtained, in contrast to conventional acousto-optic phase grating effects.

I. INTRODUCTION

WE report the observation of strong photoacoustic effects in molecular crystals, and particularly the observation of an acousto-optic *amplitude* grating effect, obtained while applying the picosecond transient grating method to the study of energy migration processes in molecular crystals.

The details of our transient-grating method and of the energy migration studies have been given elsewhere [1], [2], but it may be appropriate to briefly review the transient grating concept. Two coherent, time-coincident picosecond excitation pulses are transmitted through an experimental sample which is absorbing at the excitation wavelength, as in Fig. 1. In the experiment described here the absorbers consist of organic molecules (pentacene) imbedded in a transparent crystalline host (p-terphenyl). Optical absorption in the interference pattern between the two excitation beams produces a volume grating pattern of electronic singlet excited states of the pentacene molecules. This excited-state grating then acts as an optical absorption grating or "transient hologram." The time-dependent decay of the excited-state grating is probed by Bragg diffraction of a weak, variably delayed picosecond probe pulse. The intensity of the diffracted probe pulse is monitored as a function of probe pulse delay. In the case at hand, the grating pattern decays through a combination of excited-state decay and excited-state transport (which washes out the grating fringes). For purely diffusive excited-state energy transport, the decay is exponential, and the decay rate gives the transport parameters directly. A diffusion coef-

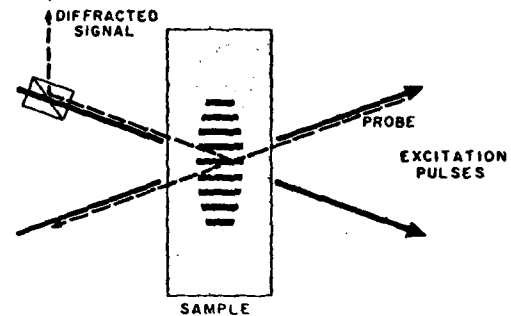


Fig. 1. Transient grating concept and geometry. Probe pulse is orthogonally polarized relative to excitation pulses, and signal is extracted with cube polarizer.

ficient for the singlet excited electronic states of pentacene in p-terphenyl has thus been obtained [2].

When we performed the same experiments at optical excitation intensities above $\sim 500 \text{ MW/cm}^2$, a strong well defined oscillatory behavior in the scattering efficiency versus decay was observed. In this paper we interpret this oscillatory behavior as due to strong photoacoustic effects. At high excitation intensities, a significant thermal grating is superimposed on the excited-state grating. This thermal grating produces a transient disturbance which can be described as a "frozen" stress pattern plus two counterpropagating coherent microwave acoustic waves [3]. The density modulation associated with this disturbance modulates, at the microwave sound frequency, predominantly the optical absorption cross section of the pentacene excited electronic singlet states, most likely by pressure tuning the absorption line. This in turn modulates the effective depth of the excited-state grating and thus its scattering efficiency, producing an amplitude grating effect. To our knowledge, such photoacoustic amplitude grating effects have not been previously observed. They provide interesting information on phonon processes and on pressure tuning in the crystals, in addition to preserving the excited-state transport information.

II. EXPERIMENTAL OBSERVATIONS

A. Apparatus

The experimental apparatus for these studies is outlined in Fig. 2. A continuously pumped, high repetition rate, Q-switched and actively mode-locked Nd:YAG laser [4] produces bursts of mode-locked pulses, from which single pulses are selected by a LiNbO_3 Pockels cell in a Blumlein configuration. These pulses are efficiently doubled to 532 nm by a

Manuscript received November 13, 1978. This work was supported by the Air Force Office of Scientific Research.

The authors are with the Edward L. Ginzton Laboratory and the Department of Electrical Engineering, Stanford University, Stanford, CA 94305.

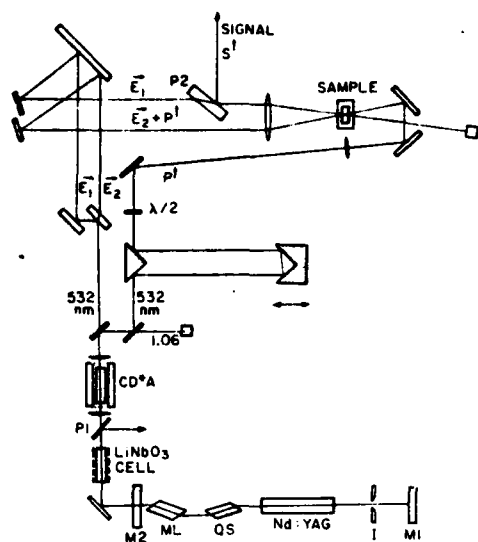
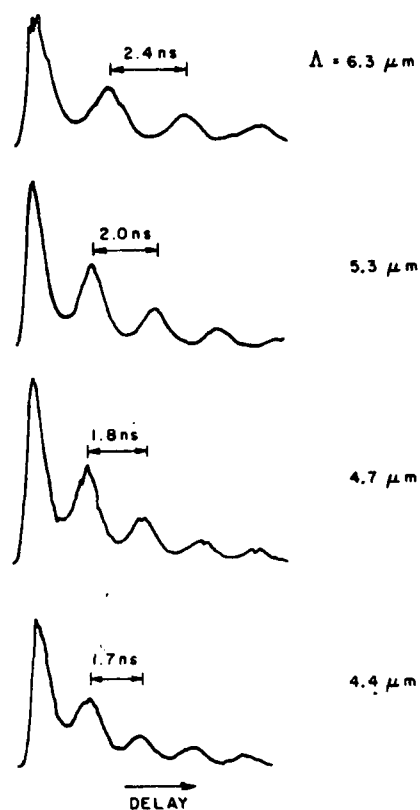


Fig. 2. Transient grating experimental setup.

temperature-tuned 90° -phase-matched CD*A crystal, and split into two strong excitation pulses (≈ 300 kW peak power each) and a weak variably delayed probe pulse (≈ 20 kW). All pulses are linearly polarized in the plane of the figure, and are Gaussian in time and in space with a duration [full width at half maximum (FWHM)] of 50–75 ps. Due to the particular optical absorption properties of pentacene at 532 nm, excitation and probe pulses are chosen to be at the same wavelength. To meet the Bragg condition, the probe pulse is brought from the back of the crystal along the reverse path of one of the excitation pulses, but with its polarization rotated by 90° . The first-order Bragg-diffracted pulse preserves this polarization and is scattered along the reverse path of the other excitation pulse. A polarization beam splitter then deflects the signal into a photodetector connected to a lock-in amplifier. The lock-in output drives the y axis of an X - Y recorder, while the x axis is driven by the motorized probe pulse delay line. For slow delay scan rate and high laser repetition rate (100 Hz), data gathering is essentially continuous in a stroboscopic sense. Each experimental plot contains typically 50 000–100 000 laser shots and takes 10 min to complete. Observed scattering efficiencies are typically several percent, yielding high signal to noise ratio in the measurements ($S/N \approx 100$ is easily achieved). To further enhance the signal discrimination, every other pair of excitation pulses is chopped and phase sensitive detection is used. A microscope objective can also be used to image the interaction volume onto a vidicon tube with large magnification, allowing the display of the grating fringes on a television monitor. This provides a very accurate tool to align all three beams in the crystal.

B. Results

Results showing diffusive energy transport at low excitation intensity have been previously reported and studied [2]. Here we concentrate on the high excitation intensity results, which show the oscillatory character of the time-dependent scattering efficiency. Fig. 3 shows this oscillatory dependence as ob-

Fig. 3. High excitation intensity transient grating results showing the dependence of the oscillation period T on the grating fringe spacing Λ , for four experimental results.

served in four experiments from a series performed under identical conditions except for different fringe spacings Λ , which are adjusted by changing the angle between the two excitation beams. In all these results the grating k vector is parallel to the crystal b axis. The time period T of the oscillatory modulation changes with fringe spacing Λ with the linear dependence shown in Fig. 4. A straight-line fit yields a slope of 2.63×10^5 cm/s, which we take to be the velocity of sound. The velocity of sound in the same crystal along the same direction was independently measured to be $v_s = 2.65 \pm 0.05$ cm/s, confirming the acoustic origin of the oscillations.

Further examination of the shape of the oscillatory decays in Fig. 3 leads us to conclude that the observed effects must result from thermal excitation of an acoustooptic amplitude grating. This grating must be produced, we believe, by acoustic pressure tuning of the excited molecular state absorption in the sample. The theoretical analysis supporting these conclusions is outlined in the following section.

III. THEORETICAL FORMULATION

A. Time Dependence of the Scattering Efficiency

The geometrical and parametric dependence of the scattering efficiency of volume holograms is well known [5], [6]. Here we are mainly interested in the exponentially decaying and oscillating time dependence of the observed scattering from the volume grating patterns produced by thermal plus excited-

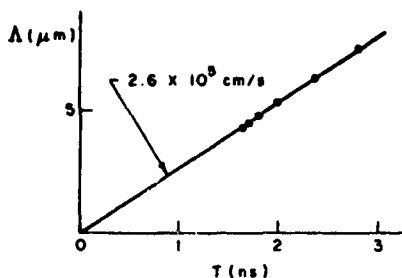


Fig. 4. Linear dependence of Λ versus T .

state gratings in our experiments. In these experiments scattered probe signals were observed primarily at the first-order Bragg-matching angle. However, the volume grating pattern also contains higher spatial harmonics, particularly at the second-order Bragg angle, which should also be observable. In general the diffracted probe signal intensity $I_n(t)$ at the n th order Bragg matching angle is given by

$$I_n(t) = \int_{-\infty}^{+\infty} I_p(t' - t) |I_e(t') * \chi_n(t')|^2 dt' \quad (1)$$

where the $*$ denotes convolution, and $I_p(t' - t)$ and $I_e(t')$ are the probe and excitation pulse intensities, with the probe pulse being delayed in time by an amount t . Out of the total complex susceptibility $\chi(x, t)$ in the sample the relevant part is the spatial Fourier component of order n , i.e., the component $\chi_n(t) \exp(jnkx)$, which corresponds to spatial vector $nk = n2\pi/\Lambda$, where Λ is the grating spacing. As written here, $\chi(x, t)$ is the Green's function or the unit impulse response produced by an excitation pulse that is a unit impulse in time. In this paper we will, in fact, treat the excitation pulse $I_e(t)$ as a unit impulse, since the ~ 70 ps excitation (and probe) pulses are short compared to the ~ 1 ns oscillation and decay times in these experiments. The scattering susceptibility $\chi_n(t)$ is in general complex, i.e., $\chi_n = \chi_n' + j\chi_n''$, with the real part being responsible for phase grating or index of refraction grating effects, and the imaginary part being responsible for amplitude or absorption grating effects.

The physical process that produces the coherent acoustic waves of interest here is a thermally induced acoustic grating which is superimposed on the excited-state grating [2]. The thermal grating and the associated acoustic waves can be analyzed starting from the linearized hydrodynamic equations [7] - [9]

$$\frac{\partial^2 \Delta \rho}{\partial t^2} + \frac{v_s^2}{\gamma} \nabla^2 \Delta \rho - \frac{\eta}{\rho_0} \frac{\partial}{\partial t} \nabla^2 \Delta \rho - \frac{v_s \beta \rho_0}{\gamma} \nabla^2 \Delta T = 0$$

$$\frac{\partial \Delta T}{\partial t} - \frac{\lambda}{\rho_0 c_v} \nabla^2 \Delta T - \frac{\gamma - 1}{\beta \rho_0} \frac{\partial \Delta \rho}{\partial t} = \frac{n c \alpha}{4 \pi \rho_0 c_v} (E_c^2) \quad (2)$$

Here ΔT and $\Delta \rho$ are the local temperature and density changes, ρ_0 is the equilibrium density, η is the viscosity, β is the expansion coefficient, λ is the thermal conductivity, α is the optical absorption coefficient, and E_c is the local optical electric field in the interaction volume. Electrostriction can be neglected, and the transient solution for the density variation $\Delta \rho$ can then be readily obtained [8] for an excitation pulse very short

compared to the acoustic times of interest:

$$\Delta \rho(x, t) = \Delta \rho_{\max} [e^{-t/\tau_{ac}} \cos \omega t - e^{-t/\tau_{th}}] \cos(2\pi x/\Lambda) \quad (3)$$

Here τ_{ac} is the acoustic wave attenuation time or sound absorption time, τ_{th} is the thermal conduction time, and $\omega = 2\pi/\tau_\Lambda$ is the acoustic frequency where $\tau_\Lambda = \Lambda/v_s$, with v_s being the acoustic wave velocity. For the acoustic frequencies generated in these experiments ($\omega/2\pi \sim 300$ -800 MHz), the acoustic decay time is $\tau_{ac} \sim 50$ -100 ns, and the thermal conduction decay time can be ignored.

A more complete analysis would take into account the Gaussian transverse spatial dependence of the excitation beams, as well as the finite duration of the excitation pulse $I_e(t)$. In particular there will be an additional effective decay of the acoustic signals as the finite trains of left- and right-going acoustic cycles move across each other and eventually cease to overlap spatially with each other. Since our gratings typically had at least 20 fringes across the half width of the beam spot size, however, this had little effect during the 5 or 6 acoustic cycles typically followed in our experiments.

Although we will speak loosely of pressure tuning effects, we attribute the observed effects in our experiments to induced changes in the local optical properties of the medium caused primarily by local density changes rather than either local temperature, local stress, or pressure effects. Fig. 5 is a plot of the excited state grating pattern $N_1(x, t=0)$, the ground state molecular density $N_0(x, t=0)$, and the instantaneous local density change $\Delta \rho(x, t)$, with the latter quantity being plotted at successive instants of time through one complete acoustic cycle, neglecting damping or decay effects. The acoustic density grating pattern is in phase spatially with the excited-state grating pattern, as well as with the sinusoidal part of the ground state molecular density. Because of the instantaneous nature of the thermal excitation in bulk, both the density and the pressure must be described as having a static or "frozen" grating component as well as two counterpropagating traveling-wave components. (The "frozen" components will of course decay away with a much longer thermal relaxation time.) Note also that the density variations with time at any one point in space are "one-sided," i.e., the local density swings up and back, or down and back, but not both up and down at any one location. The molecular densities $N_0(x)$ and $N_1(x)$ decay slowly due to excited-state relaxation and diffusion.

B. Phase Versus Amplitude Grating Effects

Conventional acoustooptic interactions in solids nearly always occur through a *phase* grating mechanism, caused by a change in local index of refraction associated with the acoustic disturbance. Examination of the theoretical expressions and of Fig. 5 shows, however, that this cannot be the primary explanation for our observations, and that we are clearly observing an acoustooptic *amplitude* grating effect.

In our results the instantaneous scattering efficiency is seen to be reduced nearly to zero at each odd half acoustic cycle after the excitation pulse. This is also the instant when the density grating reaches its maximum amplitude in spatial phase with the excited-state grating. The implication is that

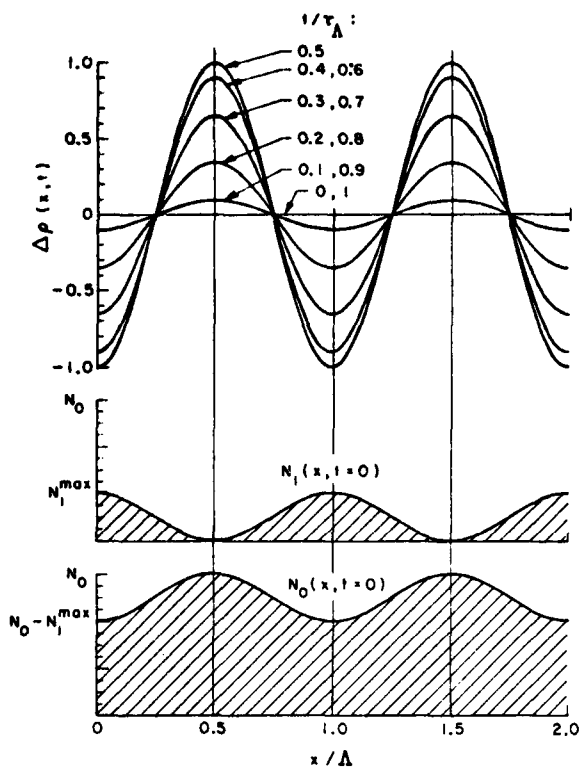


Fig. 5. Density wave dynamical behavior. Fringe peaks are at $x/\Lambda = 0, 1, 2, \dots$. Excited and ground state population spatial distribution at $t = 0$.

the density-induced scattering at those instants must add in opposite phase (not in quadrature) to the excited-state induced grating. We believe the excited-state grating must surely be an amplitude grating, and hence the density-induced grating must be an amplitude rather than a phase grating also.

Equation (3) shows that the density grating consists of two traveling-wave components of relative amplitude $+\frac{1}{2}$ each, and a fixed or constant component of relative amplitude -1 . The two traveling-wave components decay with the acoustic decay time τ_{ac} , which lasts 25-50 acoustic cycles, while the fixed component decays with the thermal decay time τ_{th} , which is much longer. Each of these components will induce a scattered signal field component at the Bragg angle, with corresponding amplitudes and phases. Note that the three density grating components, and also the three vectorial scattered wave components, sum to exactly 0 at $t = 0$ since the density modulation starts from an initial value that is identically zero.

Fig. 6 shows vectorially in the complex plane the scattered vector field amplitudes contributed by each of these three density wave components, plus the larger component contributed by the excited-state grating, at three instants of time corresponding to $0, \frac{1}{2}$, and 1 acoustic cycle. The sketches are drawn with vertical arrows representing the excited state grating, assumed to be a pure amplitude grating. The heavy arrow in each case is the vector sum, or the instantaneous vector amplitude of the total Bragg-scattered signal field. The length of this vector squared would give the total Bragg-scattered intensity at that instant.

The upper sketch assumes that the density waves induce a phase grating effect, i.e., the three acoustically induced com-

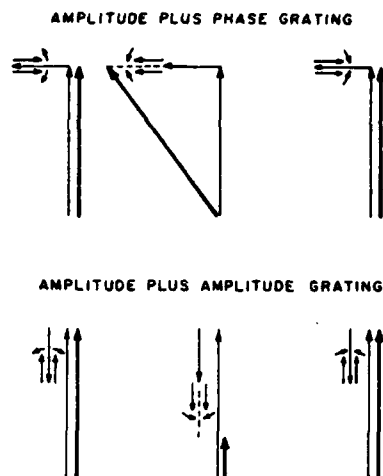


Fig. 6. Graphical (phasor) description of acoustically induced phase or amplitude grating added to excited state amplitude grating. Resultant time dependences are radically different. Only acoustically induced amplitude grating effects can explain observed time dependence.

ponents are 90° out of phase with the excited-state grating component; while the lower sketch assumes the density wave components are in phase with the excited-state component. The two smaller density wave components rotate in opposite directions in the complex plane at the acoustic frequency, since they represent oscillating or traveling-wave terms. Note that the observed amplitude variation of the total scattered signal with time can only be explained by the lower sketch. An acoustic phase grating would, in fact, cause the total scattered intensity to have an amplitude variation of opposite sign.

C. Detailed Analysis of the Scattering Efficiency

Leaving aside inessential constants and geometrical factors, the scattering susceptibility $\chi_n(t)$ can be written as

$$\chi_n(t) = j \left\{ \sum_i N_{i,\rho}(x,t) \sigma_{i,\rho}(x,t) \right\}_n \quad (4)$$

where $N_{i,\rho}$ and $\sigma_{i,\rho}$ are the density-modulated molecular state populations and cross sections, respectively, and where the subscript n indicates that only the $\exp(jn2\pi x/\Lambda)$ spatial component is to be considered. The sum in the present case extends over two levels, the ground state $i = 0$ and the first excited singlet level $i = 1$. The population and cross sections may be written as

$$\begin{aligned} N_{i,\rho}(x,t) &= N_i(x,t) [1 + \Delta\rho(x,t)/\rho_0] \\ \sigma_{i,\rho}(x,t) &= \sigma_i + (\partial\sigma_i/\partial\rho) \Delta\rho(x,t) \end{aligned} \quad (5)$$

where $N_i(x,t)$ and σ_i without arguments give the unperturbed values. The values both of σ_i and of their derivatives may in general be complex, with the real part corresponding to absorption and the imaginary part corresponding to phase shift or index of refraction effects.

The general expression for $\Delta\rho(x,t)$ has been given in (3). The populations of the ground and excited levels produced by the excitation beam delta functions are [2]

$$N_1(x, t) = \frac{1}{2} N_1^{\max} e^{-t/\tau} [1 - e^{-k^2 D t} \cos(2\pi x/\Lambda)]$$

$$N_0(x, t) = N_0 - N_1(x, t) \quad (6)$$

where N_0 without arguments is the total density of absorbing molecules in the crystal, N_1^{\max} is the initial optically induced excited-state density at the grating peaks, τ is the excited state fluorescent lifetime, and $(1/\tau + k^2 D) = K/2$ is the decay rate for the excited-state fringe pattern due to excited-state relaxation plus excited-state diffusion with diffusion coefficient D .

We now define the normalized maximum density variation

$$\eta = \Delta\rho_{\max}/\rho_0 \ll 1 \quad (7)$$

and the oscillatory modulation component

$$M(t) = \exp(-t/\tau_{ac}) \cos \omega t - 1. \quad (8)$$

We also define the cross section sensitivity parameters, or normalized density derivatives

$$S_0 = (\partial\sigma_0/\partial\rho) \rho_0/\sigma_0$$

$$S_1 = (\partial\sigma_1/\partial\rho) \rho_0/\sigma_1 \quad (9)$$

which could be complex or even imaginary if the density modulation produces an index of refraction grating. We then obtain the $n = 1$ Bragg angle component of the scattering susceptibility from (4), (8), and (9) as

$$-j\chi_1(t) = (N_1^{\max}/2) (\sigma_1 - \sigma_0) e^{-(1/\tau + k^2 D)t}$$

$$+ \eta\sigma_1 (S_1 + 1) (N_1^{\max}/2) e^{-t/\tau} M(t)$$

$$+ \eta\sigma_0 (S_0 + 1) (N_0 - (N_1^{\max}/2)) e^{-t/\tau} M(t). \quad (10)$$

This expression contains three terms. The first is the basic excited-state transient-grating signal [2] unperturbed by acoustic effects. It gives the pure exponential decay observed at low intensities, as determined by the excited-state lifetime τ and the diffusion coefficient D . The second and third terms describe how the first excited state and ground-state diffraction effects are modulated by the thermally induced density variations or coherent acoustic waves. In the $(S_i + 1)$ factors in the second and third terms, the factor of 1 represents simple density modulation of the local molecular density, while the S_i factors represent density modulation of the molecular cross sections σ_i , as in (5). It will turn out that the magnitudes of the S_i seem to be substantially larger than unity to fit the observed results.

The resulting diffracted signal intensity is then given by

$$I_1(t) = \int_{-\infty}^{+\infty} I(\rho(t' - t)) |e^{-(K/2)t'}|$$

$$+ A_1 e^{-t'/\tau} M(t')$$

$$+ A_0 (2N_0/N_1^{\max} - e^{-t'/\tau}) M(t')|^2 dt' \quad (11)$$

where we have normalized the initial scattering efficiency to unity. The oscillatory terms have magnitudes

$$A_0 = \frac{\eta(S_0 + 1) \sigma_0}{\sigma_1 \sigma_0}$$

$$A_1 = \frac{\eta(S_1 + 1) \sigma_1}{\sigma_1 \sigma_0} \quad (12)$$

Note that squaring this expression not only squares each of the above terms, but most importantly leads to beating effects between the basic excited-state grating and the two acoustic terms. Because the probe pulsewidth of ~ 70 ps is short compared to the time constants involved in $\chi_1(t)$, we can simplify (11) as

$$I_1(t) = |e^{-(K/2)t} + A_1 e^{-t/\tau} M(t)$$

$$+ A_0 (2N_0/N_1^{\max} - e^{-t/\tau}) M(t)|^2$$

$$\approx e^{-K \cdot t} + A_1 M(t) e^{-t/\tau} e^{-(K/2)t}$$

$$+ A_0 (2N_0/N_1^{\max} - e^{-t/\tau}) M(t) e^{-(K/2)t}. \quad (13)$$

Here we have also ignored products of order η^2 in the second line, since $\eta^2 \ll 1$.

Fig. 7 shows (13) plotted for typical values of the relevant time constants as we slowly "turn on" the excited-state density-modulation term A_1 and the ground-state density modulation term A_0 independently. The experimental parameters employed are

$$N_1^{\max}/N_0 = 0.3$$

$$\tau = 9.5 \text{ ns}$$

$$\tau_{ac} = 100 \text{ ns}$$

$$\Lambda = 5 \mu\text{m}$$

$$v_s = 2.65 \times 10^5 \text{ cm/s}$$

$$D = 0.5 \text{ cm}^2/\text{s}. \quad (14)$$

It clearly seems that the shape of our experimental results can be matched only by assuming that density modulation of the excited state is the dominant mechanism causing the acoustic effects. This is supported by the data shown in Fig. 8, obtained from the third plot from the top in Fig. 3. The plot shows both the exponential decay of the peak amplitudes, which gives the diffusion coefficient D , and also the decay of the depth-of-modulation amplitudes i.e., the difference between the fitting exponential and the observed amplitude at the minima. The decay rates are essentially the same, which says that the oscillatory term decays at the same rate as the grating component of $N_1(x)$, not $N_0(x)$. Only if density modulation of the excited state is the dominant mechanism can this depth of modulation decay be explained. For ground state modulation the decay would have to be significantly slower.

D. Comparison to Experimental Results

Fig. 9 repeats the experimental result of Fig. 3, second curve from the top ($\Lambda = 5.33 \mu\text{m}$), along with a semilog plot of the peak amplitudes in this curve, showing their almost exact exponential decay. At the peak times, the instantaneous density change $\Delta\rho(x, t)$ is zero, and hence the observed exponential decay rate for the peaks should be $(2/\tau + 2k^2 D)$. The observed results are in fact in agreement with low-intensity, nonoscillating measurements which give $\tau = 9.5$ ns and $D = 0.5$ cm^2/s for this particular sample. Also shown in Fig. 9 is a theoretical fit using (13) for these experimental conditions, with $A_0 = 0.02$ and $A_1 = +0.37$. Evidently it is density modulation of the excited rather than the ground level that is dominant.

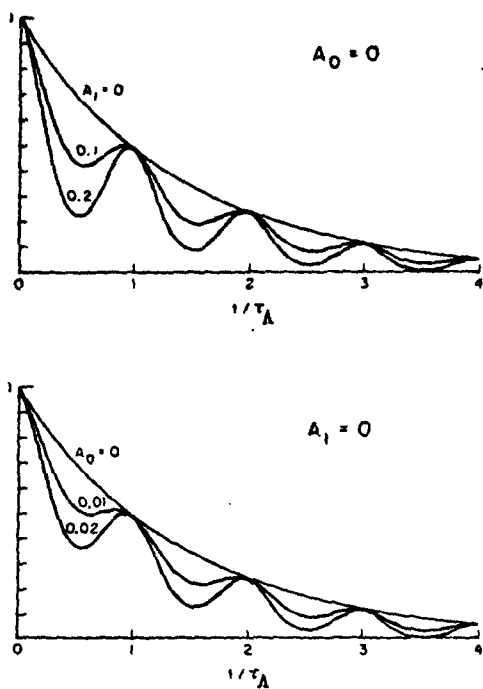


Fig. 7. Excited state (upper) modulation and ground state (lower) modulation, for several modulation "depths" A_1 and A_0 . Although behavior may look similar, the oscillation decay is radically different, being much slower for ground state modulation.

From all our other measurements, we can estimate that $\sigma_1/\sigma_0 \approx 5$, and from the heat deposition and thermoacoustic properties of the material, we can estimate that in the high intensity experiments, the normalized maximum density change corresponds to $\eta \sim 10^{-3}$. From (12) we then obtain the rough values

$$(S_0 + 1) \sim -100$$

$$(S_1 + 1) \sim +500$$

$$\frac{\Delta\sigma_0}{\sigma_0} \sim +0.05$$

$$\frac{\Delta\sigma_1}{\sigma_1} \sim -0.5 \quad (15)$$

at the peak of the acoustic wave (where $\Delta\rho/\rho_0 < 0$). There is independent support for the assumption that $\partial\sigma_0/\partial\rho < 0$, if we consider the ground state absorption spectrum of pentacene in the vicinity of 532 nm, and a static pressure tuning study of pentacene lines [10]. No data on the pressure tuning of the first singlet excited state of pentacene seem to be available, but our results imply that the net effect at 532 nm must be of opposite sign, and several times larger. The agreement shown in Fig. 9 is good, especially if we look at the simplicity of the theoretical model, in which we did not include highly nonlinear effects potentially present in the interaction volume, such as the following.

1) In the high compressibility regime produced by the laser induced acoustic waves (excess pressure ≈ 50 atm), the sound velocity can no longer be considered constant [11], and the acoustic waves can no longer be rigorously treated by a linearized model.

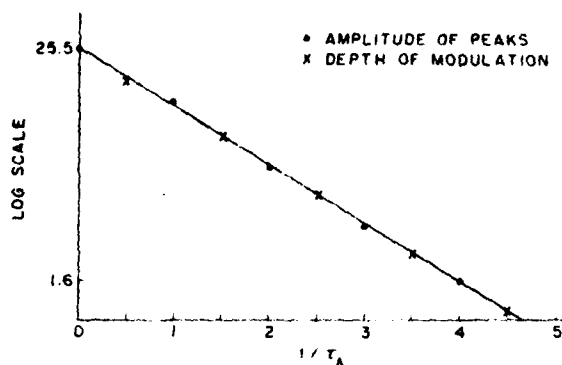


Fig. 8. •-Peak amplitudes for third plot in Fig. 3 ($\lambda = 4.7 \mu\text{m}$), showing excellent exponential decay. Decay time constant gives $D = 0.5 \text{ cm}^2/\text{s}$ for this particular sample, for diffusion along the b axis. X-Depth of modulation points obtained from minima of same plot. Observed decay can only be explained if an acoustic modulation of excited state optical properties is assumed. Ground state modulation would produce a much slower decay.

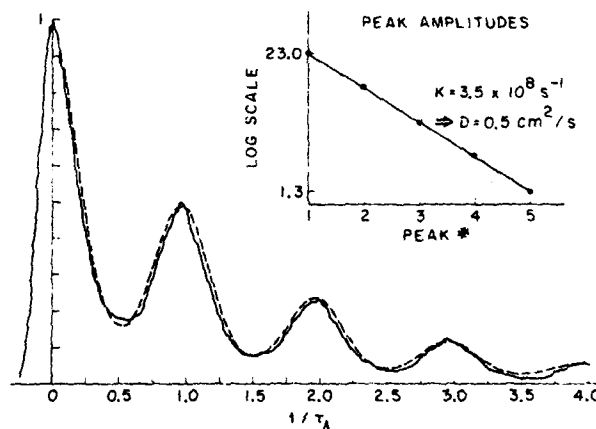


Fig. 9. Theoretical fit to second experimental plot in Fig. 3 ($\lambda = 5.3 \mu\text{m}$), for $A_0 = -0.02$ and $A_1 = +0.37$.

2) A linear dependence of cross section on density has been assumed, when in more rigor we should use the exact nonlinear absorption lineshape around 532 nm.

However, we believe including these nonlinear effects would only change the fit in Fig. 9 by a negligible amount, and in the right direction for an even more exact fit.

IV. CONCLUSION

The present paper reports the observation of amplitude grating effects produced by coherent acoustic waves induced by optical absorption of picosecond pulses. These pulses form overlapping transient excited-state and thermal gratings in the bulk of a molecular crystal. A simple model introduced to treat the coherent acoustooptic interaction fits the experimental results with quite good agreement. The results yield information about a variety of processes, including:

1) The nature and rate of energy migration for the molecular excited states, obtained by studying the decay of the oscillatory signal peaks.

2) Information regarding high-frequency acoustic phonon processes in the crystal, including acoustic velocity and attenuation. By changing the grating orientation in the crystal,

anisotropic and nonlinear acoustic effects might also be directly studied.

3) Information regarding the pressure or density modulation of the ground-state and excited-state absorption in the crystal.

The amount of information simultaneously obtained from measurements such as these, concerning both molecular and crystalline properties, is sizable. We hope this process can be naturally extended to other materials as well, providing a unified understanding of their properties.

ACKNOWLEDGMENT

Earlier work on the transient grating experiments was supported by the Joint Services Electronics Program at Stanford University and by the National Science Foundation. This work grew out of studies of energy transport in pentacene carried out in collaboration with Prof. M. Fayer and D. Dlott of the Stanford Chemistry Department, and we appreciate the use of molecular crystal samples provided by them.

REFERENCES

- [1] D. W. Phillion, D. J. Kuizenga, and A. E. Siegman, "Subnanosecond relaxation time measurements using a transient induced grating method," *Appl. Phys. Lett.*, vol. 27, pp. 85-87, 1975.
- [2] J. R. Salcedo, A. E. Siegman, D. D. Dlott, and M. D. Fayer, "Dynamics of energy transport in molecular crystals: The picosecond transient grating method," *Phys. Rev. Lett.*, vol. 41, pp. 131-133, July 10, 1978; also in *Picosecond Phenomena*, C. V. Shank, E. P. Ippen, and S. L. Shapiro, Eds. Berlin: Springer Series in Chem. Phys., vol. 4, 1978, pp. 240-243.
- [3] D. C. Auth, "New high-power source of coherent microwave phonons," *Appl. Phys. Lett.*, vol. 16, pp. 521-523, June 15, 1970.
- [4] D. W. Phillion, "Evolution of mode-locked pulses and their application to time-resolved spectroscopy," Ph.D. dissertation, Stanford Univ., Stanford, CA, Nov. 1974.
- [5] H. Kogelnik, "Coupled wave theory for thick hologram gratings," *Bell Syst. Tech. J.*, vol. 48, pp. 2909-2947, 1969.
- [6] A. E. Siegman, "Bragg diffraction of a Gaussian beam by a crossed-Gaussian volume grating," *J. Opt. Soc. Amer.*, vol. 67, pp. 545-550, 1977.
- [7] D. R. Dean, "Optically induced diffraction gratings in liquids and solids," Office of Naval Research, Washington, DC, Tech. Rep. TR-73-02.
- [8] M. E. Mack, "Stimulated thermal Rayleigh scattering with picosecond pulses," *Ann. N.Y. Acad. Sci.*, vol. 168, pp. 419-436, 1970.
- [9] R. Herman and M. Gray, "Theoretical prediction of the stimulated thermal Rayleigh scattering in liquids," *Phys. Rev. Lett.*, vol. 19, pp. 824-827, 1967.
- [10] J. M. Donnini, "Effect d'une compression sur les spectres de l'anthracène et du pentacene en solution dans le p-terphenyle a 1.7 K," *J. Chim. Phys.*, II, vol. 11-12, pp. 1542-1545, 1974.
- [11] H. Eichler and H. Stahi, "Time and frequency behavior of sound waves thermally induced by modulated laser pulses," *J. Appl. Phys.*, vol. 44, pp. 3429-3435, Aug. 1973.

Diffraction-Biased Unstable Ring Resonators with Possible Applications in Laser Gyroscopes

SHINAN-CHUR SHENG

Abstract—The performance of laser gyroscopes is seriously limited at present by the lock-in phenomenon that occurs between the counter-propagating waves at low rotation rates or low values of the beat frequency between the two waves. To minimize or eliminate this lock-in phenomenon, different techniques such as mechanical dither and Faraday cell nonreciprocal-phase elements have been proposed and studied. Here a new idea is presented, which shows how nonreciprocal propagation and a zero-rotation-rate frequency offset can be obtained by a “diffraction-bias” technique employing differential spatial filtering in a negative-branch unstable ring resonator.

I. INTRODUCTION

WE PROPOSE here a basic new technique for obtaining a zero-rotation-rate frequency offset between the counter-propagating waves in a ring laser by using a “diffraction-bias” technique in a negative-branch unstable resonator. Whether this will represent a useful technique remains to be seen. However, it does appear to provide a fundamentally new attack on the important problem of providing a frequency offset, and eliminating the lock-in problem for ring laser gyroscopes [1] at very low rotation rates.

The general structure of a negative branch unstable ring resonator with a separate focus for the mode propagating in each direction is shown in Fig. 1. To explain the basic princi-

Manuscript received March 5, 1979; revised March 15, 1979. This work was supported by the Air Force Office of Scientific Research.

The author is with Edward L. Ginzton Laboratory, Stanford University, Stanford, CA 94305.

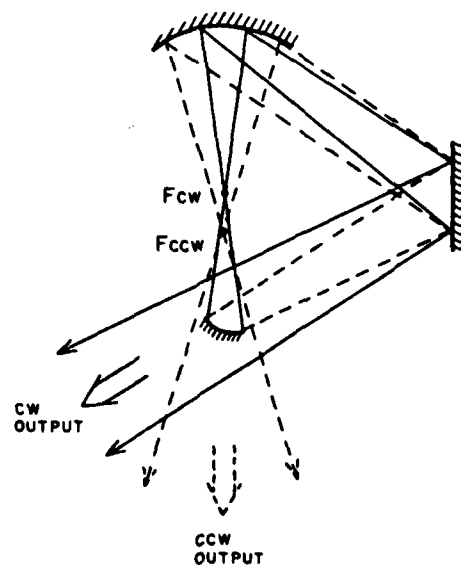


Fig. 1. A typical negative-branch unstable ring resonator.

ple of nonreciprocal-diffraction filtering, an unstable resonator with cylindrical symmetry along the optical path is assumed. Discussion of the problem of astigmatism is deferred to later in this paper.

In Fig. 1 the clockwise (CW) propagation wave has a focus at F_{CW} , while the counter-clockwise (CCW) wave has one at

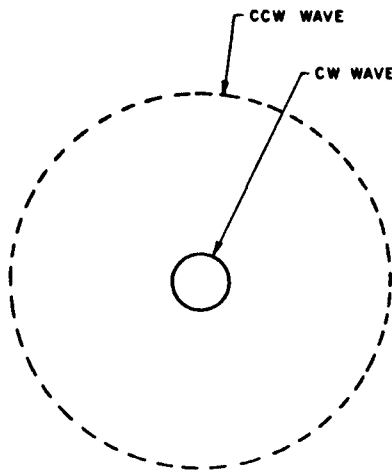


Fig. 2. Schematic representation of transverse dimensions of CW and CCW waves at the CW focal plane F_{CW} .

F_{CCW} . In general F_{CW} and F_{CCW} do not have the same location in a negative-branch ring unstable cavity. If proper design is used (e.g., equivalent Fresnel number $N_{eq} \approx 0.5, 1.5, 2.5 \dots$, where the higher order transverse modes are well separated, plus appropriate intracavity apertures, etc.), the CW and CCW waves will both oscillate in the lowest transverse mode, with azimuthal symmetry parameter $l = 0$.

At the focal plane containing the focus F_{CW} , the transverse dimensions of the CW and CCW waves are different, as shown in Fig. 2. At the other focal plane containing F_{CCW} , the situation is just reversed, with the CCW wave small at the center and the CW wave larger.

Suppose we insert two fine pins at the focal plane F_{CW} as shown in Fig. 3 in such a manner that they are not deep enough to disturb the CW wave propagation, but they do penetrate into the region that the CCW wave occupies. This "differential-spatial filtering" will cause the CCW wave to suffer very high diffraction loss in the $l = 0$ mode, and hence the allowed oscillations in that direction can only be the modes with $l = 1, 2, 3, \dots$.

Usually, higher l azimuthal modes have larger transverse dimensions. So, an aperture at the focal plane F_{CW} can restrain the CCW wave from oscillating in $l \geq 2$ azimuthal modes. Similarly a proper aperture at the focal plane F_{CCW} can stop any $l \geq 1$ oscillation of the CW wave.

If instead of two pins we put in 4, 6, 8 \dots pins at equal angles¹ we may be able to force the lowest azimuthal mode of the CCW wave to run in $l = 2, 3, 4 \dots$, respectively.

Similarly, a pin diffraction filter can be placed at focal plane F_{CCW} to obtain forced higher azimuthal mode oscillation of the CW wave. If CW and CCW waves are operating in different l modes, then the roundtrip phase shifts will be nonreciprocal in the two directions, and a frequency offset of "diffraction-

¹ "Diffraction bias" is not limited to azimuthal filtering only. In fact, any selective filtering mechanism which differentially enhances certain transverse modes (radial or azimuthal, x or y) in one direction is applicable.

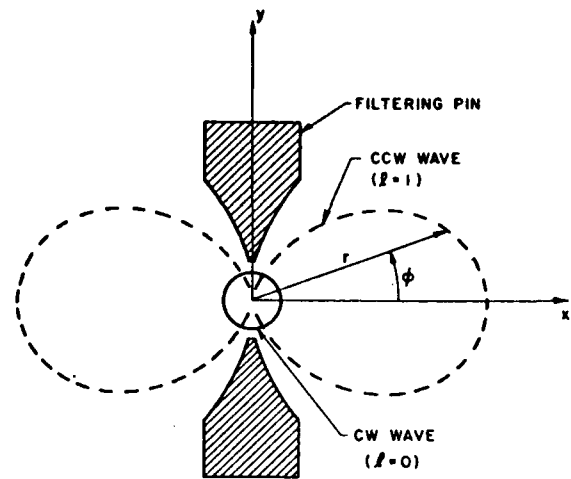


Fig. 3. Illustration of differential-spatial filtering, forcing oscillation in $l = 1$ for the CCW wave, while allowing $l = 0$ oscillations for the CW wave.

biased" beat frequency will result even a zero rotation rate of the laser cavity.

Let θ_{CW} and θ_{CCW} be the roundtrip phase shifts of the CW and CCW waves, L be the roundtrip optical path length, and λ_{CW} and λ_{CCW} be the optical wavelengths in the laser medium. We can find that the frequency difference of the CW and CCW waves when they are not in physical rotation, i.e., the dc bias beat frequency due to nonreciprocal-diffraction filtering, will be given by

$$\left(\frac{2\pi L}{\lambda_{CW}} + \theta_{CW} \right) - \left(\frac{2\pi L}{\lambda_{CCW}} + \theta_{CCW} \right) = 2\pi n \quad (1)$$

or

$$\begin{aligned} \Delta\nu &\equiv (\nu_{CW} - \nu_{CCW})_{\text{no rotation}} \\ &= \frac{c'}{L} \left[n - \frac{(\theta_{CW} - \theta_{CCW})}{2\pi} \right] \end{aligned} \quad (2)$$

where c' is the speed of light inside the resonator, and n is the integer difference between axial mode numbers of the two waves. The lowest beating frequency between the two closest waves is obtained by choosing the proper n which minimizes $|\Delta\nu|$.

We may call this scheme "diffraction bias" as compared to "Faraday cell bias" or "mechanical bias." This constant diffraction bias may be able to get rid of the lock-in phenomenon, in exactly the same way as a Faraday cell does in some laser gyroscopes.

This diffraction bias has the following properties.

1) An intracavity Faraday cell can cause problems like bias shifting, etc., if there are magnetic field or temperature variations. Diffraction bias may be insensitive to changes in external physical parameters, which means better and more stable gyroscope performance can be achieved.

2) Compared to both mechanical dither and Faraday cell bias, diffraction bias may be simpler in construction and perhaps easier in maintenance.

Astigmatism is an effect of some concern in ring laser design.

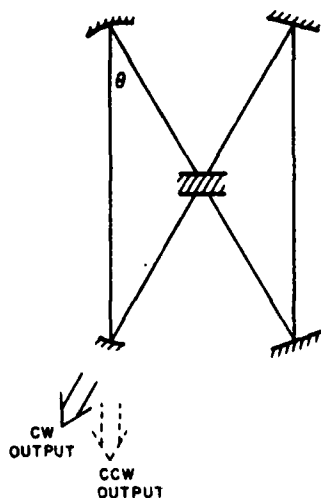


Fig. 4. With designs such as the above, keeping all angles of incidence $\theta < 15^\circ$, astigmatism generally will be small.

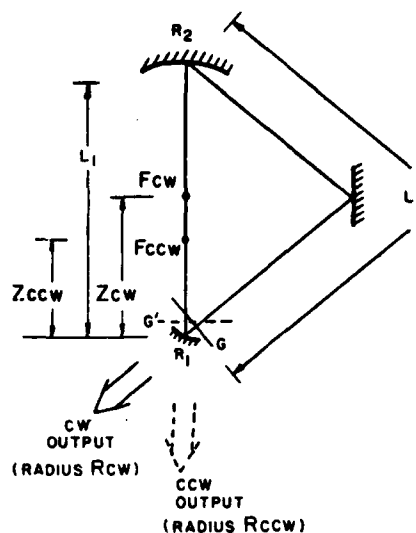


Fig. 5. General nomenclature for a simple negative branch unstable resonator.

If astigmatism is serious, we may use either aspherical mirrors or a small-angle design like Fig. 4 to minimize its effect. Even with astigmatism our former discussion is still true, i.e., there are still nonoverlapping focal points and hence differential-spatial filtering is still applicable and bias can be obtained through proper implementation of filtering pins.²

II. GEOMETRICAL ANALYSIS OF UNSTABLE RING RESONATORS

We will first develop a geometrical analysis to predict the locations of the focal points in an unstable ring resonator. Let L_1, L_2 be the separation lengths of two mirrors with radius of curvature R_1 and R_2 , respectively, as shown in Fig. 5. For the CW wave, we choose a reference plane G right before the output coupler R_1 . The roundtrip $ABCD$ matrix elements for the propagation sequence $G \rightarrow R_1 \rightarrow L_1 \rightarrow R_2 \rightarrow L_2 \rightarrow G$ are then as follows:

$$\begin{aligned} A_{CW} &= \left(1 - \frac{2L_2}{R_2}\right) \left(1 - \frac{2L_1}{R_1}\right) - \frac{2L_2}{R_1} \\ B_{CW} &= \left(1 - \frac{2L_2}{R_2}\right) L_1 + L_2 \\ D_{CW} &= 1 - \frac{2L_1}{R_2} \end{aligned} \quad (3)$$

At plane G the diverging, perturbation-stable geometric eigenmode [2] is a spherical wave with radius of curvature R_{CW} given by

$$\frac{1}{R_{CW}} = \frac{1}{B} \left[-\frac{(A-D)}{2} \pm \sqrt{\left(\frac{A+D}{2}\right)^2 - 1} \right]. \quad (4)$$

²The astigmatism mentioned here is mainly due to tilted mirrors, where the cylindrical symmetry along the optical path is spoiled. As a result we have 2 two fold symmetry with one symmetry axis in the plane of the ring and the other perpendicular to it. This indicates at least two pins can be put along either axis to induce nonreciprocal eigenmodes.

If $R_{CW} > 0$, the wave is divergent in the direction of travel.

The CW wave is focused down to the focal point F_{CW} after reflection off the output mirror R_1 . The distance Z_{CW} from R_1 to F_{CW} along path L_1 is given by

$$\frac{1}{Z_{CW}} + \frac{1}{R_{CW}} = \frac{2}{R_1} \quad (5)$$

or

$$Z_{CW} = \frac{R_1 R_{CW}}{2R_{CW} - R_1} \quad (6)$$

assuming that $0 \leq Z_{CW} \leq L_1$, so that F_{CW} is within the L_1 segment. If F_{CW} falls outside this range, the additional focusing effect of mirror R_2 must be taken into account. (It is also possible to have 3, 5, ... foci in a more complicated multielement negative-branch unstable resonator, but here we are only interested in the single-focus case.)

For the CCW wave the reference plane is set at G' and all the former calculations are valid with the exchange of L_1 and L_2 . The CCW focus F_{CCW} is now located at $R_{CCW}/2$ behind the output mirror.

A typical example, with confocal design in the CW direction but not in the CCW direction, is the following:

$$R_1 = 18 \text{ cm}$$

$$R_2 = 24 \text{ cm}$$

$$L_1 = 21 \text{ cm}$$

$$L_2 = 50.5 \text{ cm}$$

$$Z_{CW} = 9 \text{ cm (on } L_1 \text{ from } R_1)$$

$$Z_{CCW} = 6.9 \text{ cm (on } L_1 \text{ from } R_1)$$

$$\lambda = 1.15 \mu \text{ (or } 3.39 \mu)$$

$$2a = 2 \text{ mm (or } 3.43 \text{ mm for } 3.39 \mu) \\ \text{(output coupler diameter)}$$

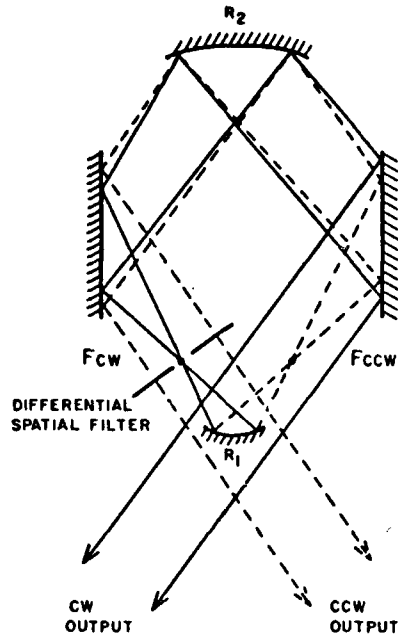


Fig. 6. Example of a symmetric confocal design.

$$M = -\frac{4}{3}$$

$$N_{eq} = 1.5.$$

The locations of F_{CW} , F_{CCW} are then as shown in Fig. 5. The two foci are separated by a distance of 2.1 cm.

To obtain larger focal separation, a symmetric confocal design as shown in Fig. 6 may be used. At these focal points, there is larger mode area difference between the CW and CCW waves (see following analysis), which allows easier and more efficient nonreciprocal filtering to exist.

III. DIFFRACTION EIGENMODE ANALYSIS

We now develop a full diffraction analysis of the CW and CCW eigenmodes for a typical example. The full eigenmode integral equation for the unstable resonator with roundtrip A, B, C, D matrix element is³

$$\begin{aligned} \gamma E(X', Y') = & \frac{j e^{-jkL}}{\lambda \sqrt{|B_x B_y|}} \iint E(X_0, Y_0) \\ & \cdot \exp \left[-j \frac{\pi}{B_x \lambda} (A_x X_0'^2 - 2X'X_0' + D_x X_0'^2) \right] \\ & \cdot \exp \left[-j \frac{\pi}{B_y \lambda} (A_y Y_0'^2 - 2Y'Y_0' + D_y Y_0'^2) \right] \\ & \cdot dx_0' dy_0'. \end{aligned} \quad (7)$$

If we assume cylindrical symmetry $E(X', Y') = \mathcal{E}_l(r') \cdot e^{+jl\phi}$, and change to Hankel transforms, we have

³The propagation phasor is assumed to be $e^{-jk \cdot \vec{r}}$. If $e^{+jk \cdot \vec{r}}$ is given, all signs associated with j should be changed.

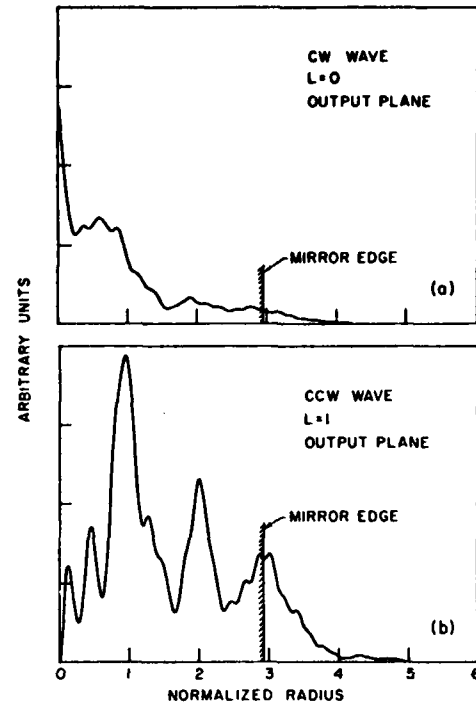


Fig. 7. (a) Intensity of the CW $l=0$ eigenmode versus radius (in normalized coordinates) at the reference plane just inside the output coupler. (b) Intensity of the CCW $l=1$ eigenmode along $\phi=0$ radius at the other reference plane just inside the output coupler.

$$\begin{aligned} \gamma \mathcal{E}_l(r) = & \exp \left[-j \left(kL - \frac{\pi}{2} \right) \right] \cdot \exp [-j\pi D r^2] \cdot (tj)^l 2\pi \\ & \cdot \int_0^{a/\sqrt{|B|\lambda}} \mathcal{E}_l(r_0) \exp [-j\pi A r_0^2] \\ & \cdot J_l(2\pi r r_0) r_0 dr_0 \end{aligned} \quad (8)$$

where L = roundtrip optical length, a = output coupler radius

$$r \equiv \frac{r'}{\sqrt{|B|\lambda}}, r_0 \equiv \frac{r_0'}{\sqrt{|B|\lambda}}, t = \text{sgn}(B)$$

and $l = 0, 1, 2, 3, \dots$ is the azimuthal symmetry number. The extra phase shift $(tj)^l$ is particularly important in determining the diffraction-bias beat frequency. A symmetric confocal design (Fig. 6) was tested using a standard resonator program with the following parameters:

$$\left. \begin{aligned} A &= -\frac{R_2}{R_1} \\ B &= L_1 \left(1 - \frac{R_1}{R_2} \right) \\ D &= \frac{1}{A} \end{aligned} \right\} \quad (9)$$

$$L_1 = L_2 = 41 \text{ cm}$$

$$R_1 = 35 \text{ cm}$$

$$R_2 = 47 \text{ cm}$$

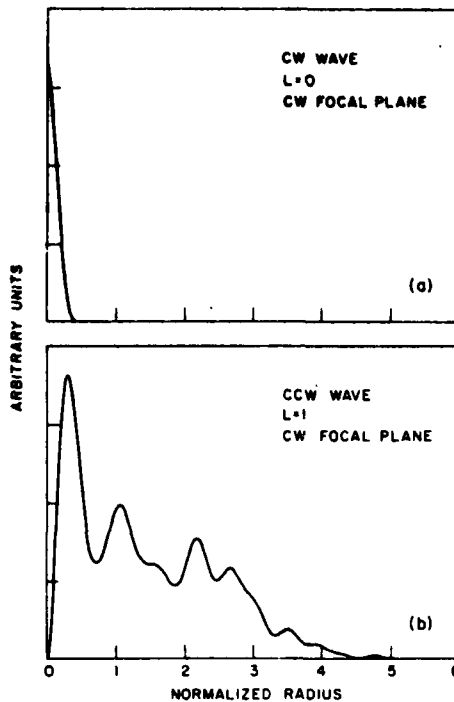


Fig. 8. (a) Intensity of the CW $l=0$ eigenmode versus radius at the CW focal plane F_{CW} . (b) Intensity of the CCW $l=1$ eigenmode along $\phi=0$ radius at the same F_{CW} plane.

$$a = 1 \text{ mm (or } 1.72 \text{ mm for } 3.39 \mu\text{)}$$

$$\lambda = 1.15 \mu \text{ (or } 3.39 \mu\text{)}$$

$$Z_{CW} = Z_{CCW} = 17.5 \text{ cm}$$

$$M = -\frac{4}{3}$$

$$N_{eq} = -2.5.$$

It was assumed that as a result of spatial filtering the collimated CW wave was operating in the $l=0$ mode, and the collimated CCW wave was filtered and operating in the $l=1$ mode. An iterative computer program written with the fast Hankel transform (FHT) algorithm [3] was used to find the CW and CCW eigenmodes, which are shown in Fig. 7. (Each mode required about 70 iterations to reach the convergence level of $|\Delta\gamma| < 10^{-3}$.) The mode patterns at the CW and CCW foci are also illustrated in Figs. 8 and 9. These clearly show that the sizes of these two waves are significantly different, as expected. Spatial filtering by inserting two pins to constrain the CCW wave but not the other should definitely be possible. The associated complex eigenvalues in the two directions are found to be

$$|\gamma_{CW}(l=0)| = 0.888$$

$$\theta_{CW}(l=0) = 1.5660$$

$$|\gamma_{CCW}(l=1)| = 0.846$$

$$\theta_{CCW}(l=1) = 3.0013 + \frac{\pi}{2}.$$

The two oppositely directed modes do not have exactly the same losses but the losses are close enough that simultaneous oscillation in the two directions at least seems conceivable, perhaps with further adjustment of the resonator parameters

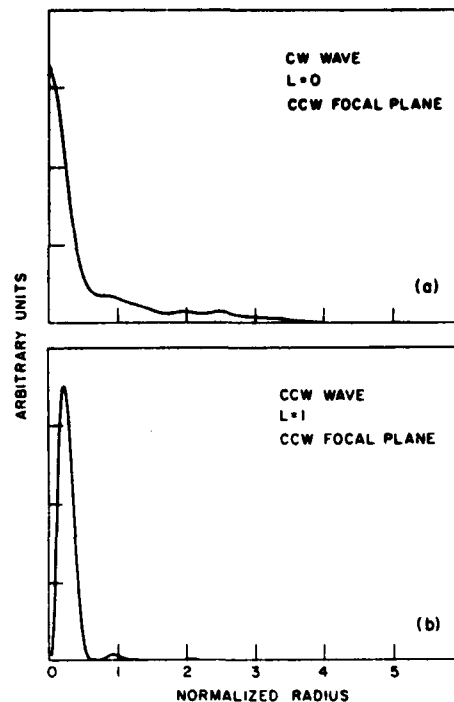


Fig. 9. (a) Intensity of the CW $l=0$ eigenmode versus radius at the CCW focal plane F_{CCW} . (b) Intensity of the CCW $l=1$ eigenmode along $\phi=0$ radius at the same F_{CCW} plane.

The extra $\pi/2$ of θ_{CCW} is due to the phase factor $(\eta)^l$ in (8), which was not included in the resonator program. The diffraction-biased beat frequency for this case is $\Delta\nu \approx 176$ MHz. Different cavity parameters (e.g., R_1, R_2, L_1, L_2, l) were also tried, and beat frequencies ranging from a few megahertz to several gigahertz were obtained. More systematic information on the variations of transverse beat frequencies in unstable resonators would be useful in this connection.

IV. CONCLUSION

The idea of using differential-spatial filtering or "diffraction bias" in negative-branch unstable ring resonators to obtain nonreciprocal oscillation frequencies appears to be a new idea. The potential application of this technique in laser gyroscopes is particularly interesting. More work is needed to see what further practical advantages, or disadvantages, are associated with this technique.

ACKNOWLEDGMENT

I appreciate Prof. A. E. Siegman's patience in reading and correcting the manuscript.

REFERENCES

- [1] F. Aronowitz, "The laser gyro," in *Laser Applications*, vol. 1, M. Ross, Ed. New York and London: Academic, 1971.
- [2] A. E. Siegman, "A canonical formulation for analyzing multielement unstable resonators," *IEEE J. Quantum Electron.*, vol. QE-12, pp. 35-40, Jan. 1976.
- [3] "Quasi fast Hankel transform," *Opt. Lett.*, vol. 1, pp. 13-15, July 1977.
- [4] R. J. Freiberg, P. P. Chenausky, and C. J. Buczek, "Unidirectional unstable ring lasers," *Appl. Opt.*, vol. 12, pp. 1140-1144, June 1973.
- [5] P. Dal Pozzo, R. Polloni, O. Svelto, and F. Zappa, "An unstable ring resonator," *IEEE J. Quantum Electron.*, vol. QE-9, pp. 1061-1063, Nov. 1973.

Quasi fast Hankel transform

A. E. Siegman

Edward L. Ginzton Laboratory and Department of Electrical Engineering, Stanford University, Stanford, California 94305
 Received March 25, 1977

We outline here a new algorithm for evaluating Hankel (Fourier-Bessel) transforms numerically with enhanced speed, accuracy, and efficiency. A nonlinear change of variables is used to convert the one-sided Hankel transform integral into a two-sided cross-correlation integral. This correlation integral is then evaluated on a discrete sampled basis using fast Fourier transforms. The new algorithm offers advantages in speed and substantial advantages in storage requirements over conventional methods for evaluating Hankel transforms with large numbers of points.

In many optical calculations one would like to evaluate Hankel transforms numerically with computational efficiency analogous to the fast Fourier transform. We describe here a new "fast Hankel transform" (FHT) algorithm that can evaluate Hankel transforms while providing many of the desired benefits.

The standard Hankel transform of order l is given by

$$g(\rho) = 2\pi \int_0^{\infty} r f(r) J_l(2\pi\rho r) dr \quad (1)$$

with a symmetric reverse transform integral from $g(\rho)$ to $f(r)$. Using the change of variables $r = r_0 e^{\alpha x}$, $\rho = \rho_0 e^{-\alpha y}$, where r_0, ρ_0 , and α are initially arbitrary, converts the one-sided Hankel transform integral [Eq. (1)] into the two-sided cross-correlation integral

$$\hat{g}(y) = \int_{-\infty}^{\infty} \hat{f}(x) \hat{j}(x+y) dx, \quad (2)$$

in which the input and transform functions are $\hat{f}(x) = rf(r)$, $\hat{g}(y) = \rho g(\rho)$, and the modified Bessel kernel is $\hat{j}(x+y) = 2\pi\alpha r\rho J_l(2\pi r\rho)$. This change of variables might be called the "Gardner transform."¹ It has been applied elsewhere to exponential or Laplace transforms^{2,4} and can potentially be applied to any integral transform whose kernel has a product argument.⁵

A correlation integral such as Eq. 2 can be evaluated efficiently in a discrete sampled approximation by using Fourier-transform methods. Sampling the functions $\hat{f}(x)$ and $\hat{g}(y)$ at discrete values given by $x = n$, $y = m$ with $n, m = 0, 1, \dots, N-1$ is equivalent to sampling the original functions $f(r)$ and $g(\rho)$ at discrete exponentially increasing values given by

$$r_n = r_0 e^{\alpha n}, \quad \rho_m = \rho_0 e^{-\alpha m}. \quad (3)$$

These sampled values are confined to truncated ranges $r_0 \leq r < b$ and $\rho_0 \leq \rho < \beta$ with upper limits $b = r_0 e^{\alpha N}$ and $\beta = \rho_0 e^{-\alpha N}$. The product βb is a space-bandwidth product for the transform. In terms of the sampled values $\hat{f}_n = \hat{f}(x_n) = r_n f(r_n)$, $\hat{g}_m = \hat{g}(y_m) = \rho_m g(\rho_m)$, and $\hat{j}_{n+m} = \hat{j}(x_n + y_m) = 2\pi\alpha r_n \rho_m J_l(2\pi r_n \rho_m)$, the Hankel transform integral [Eq. (1) or Eq. (2)] is approximated to some level of accuracy by the discrete sum

$$g_m = \sum_{n=0}^{N-1} \hat{f}_n \hat{j}_{n+m}. \quad (4)$$

If the input sequence \hat{f}_n is padded with zeros and the upper limit of the sum extended to $2N-1$, this sum becomes a $2N$ -term discrete circular correlation. This discrete correlation can be evaluated exactly using the discrete $2N$ -term fast Fourier transforms of the input sequences \hat{f}_n and \hat{j}_n by carrying out the steps

$$g_m = \text{FFT} [\text{FFT}(\hat{f}_m) \times \text{FFT}^*(\hat{j}_m)]. \quad (5)$$

The FFT and FFT* notations indicate the forward and inverse ($\pm j$) Fourier transforms (or vice versa). The two FFT's inside the brackets are multiplied together term by term before performing the outer FFT.

To the extent that the values g_m generated by Eq. (4) or Eq. (5) represent a good approximation to the true sampled transform values $\hat{g}(y_m)$, this procedure computes an N -point discrete approximation to a Hankel transform by computing two $2N$ -term fast Fourier transforms plus $2N$ additional multiplications. The transforms are performed in place, requiring only the additional storage of $2N$ previously computed values of the Fourier transform of \hat{j}_{n+m} . The extra values of g_m from $m = N$ to $m = 2N-1$ represent aliased results from the circular correlation process and are discarded.

Criteria for choosing the parameters r_0, ρ_0 , and α can be developed as follows. If β is the largest value of ρ in the transform domain, the highest frequency component in the r domain is $J_l(2\pi\beta r) \sim \cos(2\pi\beta r)$. We then require that the lower-end truncation point in the r domain not be larger than $1/K_1$ cycles of the highest spatial frequency β , or $r_0 = (K_1\beta)^{-1}$. Similarly we require that the sample point spacing $\Delta r_n = r_{n+1} - r_n$ at the upper truncation point $r = b$ not be greater than $1/K_2$ cycles of β , or $\Delta r_N \approx \alpha b = (K_2\beta)^{-1}$. Combining these arguments with exactly analogous arguments in the ρ domain, namely $\rho_0 = (K_1 b)^{-1}$ and $\Delta \rho_N = \alpha\beta = (K_2 b)^{-1}$, leads to the set of relations

$$\begin{aligned} N &= K_2 \beta b \ln(K_1 \beta b), \\ \alpha e^{\alpha N} &= K_1 / K_2, \\ r_0 \rho_0 &= (K_2 / K_1^2) \alpha. \end{aligned} \quad (6)$$

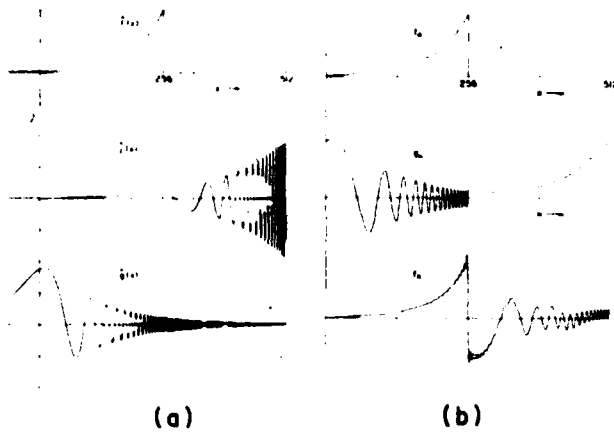


Fig. 1 (a) Exact analytical functions $f(r)$, $j(x)$, and $g(x)$ corresponding to a uniform circular "top-hat" input function $f(r)$ and its Airy-disk Hankel transform, including the top-hat input function f (top curve); the $l = 0$ Bessel-function kernel j (middle curve); and the Airy-disk Hankel transform g (bottom curve). Parameter values for the change of variables are $\alpha = 0.01612$, $r_0 = \rho_0 = 0.06349$, and $\beta = b = 3.938$, corresponding to $N = 256$, $K_1 = K_2 = 4$. The "dimples" in the g function at larger arguments are spurious results of a plotting routine with inadequate point spacing. (b) Discrete Hankel transformation and then backtransformation of a sampled top-hat input sequence f_n (top curve) into the transformed sequence g_n (middle curve) and then back into a sequence f_n (bottom curve), using the FHT algorithm with $N = 256$, $K_1 = K_2 = 4$. The portions of the transformed and backtransformed sequences g_n and f_n above $n = 256$ arise from aliasing effects in the transform algorithm and are discarded. The backtransformed sequence f_n exhibits Gibbs phenomena because of the finite truncation of the g_n sequence before it is backtransformed.

We hypothesize that the "points-per-cycle" parameters K_1 and K_2 should both be ≥ 2 points per cycle. Equations (6) then determine α , $r_0\rho_0$, and βb appropriate to a given number of points N ; or alternatively the number of points N and the α and $r_0\rho_0$ parameters required to transform with adequate accuracy a function-transform pair having a given space-bandwidth product βb .

This algorithm was programmed in FORTRAN using single-precision arithmetic on an IBM 370/168 computer. Figure 1(a) shows for purposes of comparison analytical plots of a "top-hat" input function $f(r) = 1$, $0 \leq r \leq b$, transformed into $f(x)$; the modified Bessel kernel $j(x)$; and the Airy-disk function $g(x)$ that is the exact Hankel transform of a uniform input; all plotted as continuous functions for parameter values corresponding to $l = 0$, $N = 256$, and $K_1 = K_2 = 4$ points/cycle. The kernel function $j(x)$ is seen to be slowly divergent at large x .

Figure 1(b) shows the discrete numerical results generated by the FHT algorithm for this case. The FHT algorithm samples the input function $f(x)$ [or alternatively $g(x)$] at integer values from 0 to 255, pads the input sequence with zeros from 256 to 511, performs a discrete circular convolution against 512 sampled points from the kernel $j(x)$, and yields an output sequence that approximates the exact Hankel transform

over the range 0-255 and contains aliased results over the range 256-511.

In Fig. 1(b) the middle curve shows the output sequence g_m generated by the FHT algorithm for the "top-hat" input sequence of the top curve, using $N = 256$ and $K_1 = K_2 = 4$. The Airy disk transform $g(\rho) = 2J_1(2\pi b\rho)/\rho$ is accurately reproduced by the FHT algorithm for $0 \leq m < N$, with irrelevant aliased values for $m \geq N$. The sequence g_m , when truncated and fed back through the FHT algorithm, provides a fair reproduction of the original top hat, as shown in the bottom curve; but with obvious Gibbs-phenomena ripples resulting from the finite truncation of the Airy-disk transform.

The Laguerre-Gaussian functions $u_{pl}(r) = (2\pi r)^2 L_p^l(2\pi r^2) \exp(-\pi r^2)$ are self-transforming under Hankel transformation. Figure 2 shows in r, ρ coordinates the FHT algorithm applied twice in succession to a Laguerre-Gaussian function with $l = 0$ and $p = 8$, using $N = 128$ with $K_1 = K_2 = 2$. The mean-square error on successive transforms in this case is $\leq 0.4\%$. Laguerre-Gaussians have been accurately transformed out to $p \approx 100$ for $N = 1024$, $K_1 = 8$, and $K_2 = 2$.

Figure 3 shows a top hat and also an annular function transformed and then backtransformed using the FHT algorithm. The observed Gibbs-phenomena ripples are expected for finite truncation in the transform domain whatever Hankel transform algorithm may be employed. They can presumably be reduced by using proper windowing (apodizing). The "droop" in the function values at low r is understood and can be eliminated also.

A small number of experiments indicate that the FHT algorithm works equally well for higher-azimuthal-order Hankel transforms. Beyond the preliminary tests summarized here, the capabilities of this

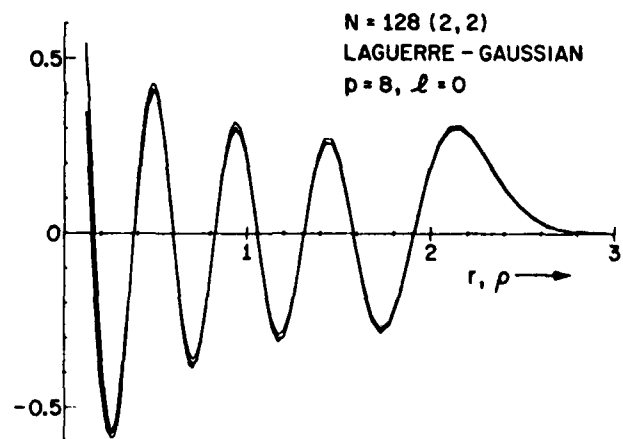


Fig. 2 The input function and two successive FHT's of a Laguerre-Gaussian input function with $p = 8$, $l = 0$ using the FHT algorithm with $N = 128$, $K_1 = K_2 = 2$. The first FHT lies essentially on top of the input function at low arguments and then drops slightly lower. The second FHT is initially slightly lower, then follows closely the first FHT. The curves are plotted as straight lines between the discrete sample points; the discrete point spacing is evident at larger arguments.

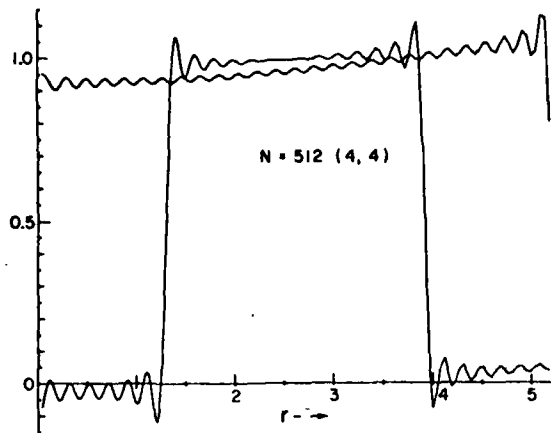


Fig. 3 Results of Hankel-transforming and then back-transforming a top-hat input function $f(r) = 1, 0 \leq r \leq b$, and a uniform annular function $f(r) = 1, b/4 \leq r \leq 3b/4$, using the FHT algorithm with $N = 512, K_1 = K_2 = 4$ ($\alpha = 0.0091648, r_0 = 0.0478665, b = 5.223$). The slump in the top-hat response and, to a lesser extent, in the annular response at low r is related to the truncation at ρ_0 of the narrow Airy-disk Hankel transform in the ρ domain; rescaling of the r and ρ coordinates to give comparable widths in the two domains gives much better results.

algorithm remain to be fully determined (and optimized). One can compare the computational efficiency of the FHT algorithm with straightforward numerical evaluation of Hankel transforms using trapezoidal integration at uniformly spaced sample points with K points per cycle in both r and ρ domains. Assuming that the Bessel function values will be stored in a look-up table, this calculation will require $N = K\beta b$ sample points in each domain and $\frac{1}{2}N^2 = \frac{1}{2}(K\beta b)^2$ complex multiplications per transform. The FHT algorithm, including the aliased values, requires a larger number $2N = 2K_2\beta b \ln(K_1\beta b)$ of sample points because of the unavoidable oversampling with exponentially spaced sample points. However, only $\sim 2N \log_2 4N$ complex multiplications are required to compute the FFT's plus additional steps in the FHT algorithm. The FHT algorithm requires significantly fewer operations for space-bandwidth products above $\beta b \approx 140$ for $K = K_1 = K_2 = 2$ or above $\beta b \approx 70$ for $K = K_1 = K_2 = 4$ points

per cycle. One might also hope to obtain improved accuracy against round-off errors because of the superior properties of the FFT algorithm, although this point has yet to be tested.

Of greatest practical importance, however, is the reduction in computer storage requirements using the FHT algorithm. Straightforward Hankel-transform evaluation using stored Bessel-function values requires storing $\frac{1}{2}(K\beta b)^2$ real values of the Bessel kernel $J_1(2\pi r\rho)$ for equally spaced values of both r and ρ (or else the use of interpolation techniques that require additional multiplications). The FHT algorithm, in contrast, is carried out in place, requiring storing only $8K_2\beta b \ln(K_1\beta b)$ total real numbers in the function and kernel arrays. For $\beta b = 1000$ and $K_1 = K_2 = 2$, this would require ~ 500 Kbytes of storage, assuming 4 bytes per real number, as against ~ 8000 Kbytes in the standard case.

These advantages in speed, storage requirements, and potential accuracy should make the FHT algorithm valuable in optical-beam and resonator calculations as well as in other optical and nonoptical applications. Further tests and improvements on the basic algorithm will be reported in future publications.

This work was carried out with support from ERDA through the Los Alamos Scientific Laboratory; from United Technology, Pratt & Whitney Aircraft; and from the Air Force Office of Scientific Research.

References

1. D. G. Gardner, J. C. Gardner, G. Lausch, and W. W. Meinke, "Method for the analysis of multi-component exponential decays," *J. Chem. Phys.* 31, 987 (1959).
2. J. Schlesinger, "Fit to experimental data with exponential functions using the fast fourier transform," *Nucl. Instrum. Methods* 106, 503 (1973).
3. M. R. Smith and S. Cohn-Sfetcu, "Comments on fit to experimental data with exponential functions using the fast fourier transform," *Nucl. Instrum. Methods* 114, 171 (1974).
4. S. Cohn-Sfetcu, M. R. Smith, S. T. Nichols, and P. L. Henry, "A digital technique for analysing a class of multicomponent signals," *Proc. IEEE* 63, 1460 (1975).
5. S. Cohn-Sfetcu, M. R. Smith, and S. T. Nichols, "On the representation of signals by basis kernels with product argument," *Proc. IEEE* 63, 326 (1975).

APPENDIX V

ORTHOGONALITY PROPERTIES OF OPTICAL RESONATOR EIGENMODES

by

A. E. Siegman

Edward L. Ginzton Laboratory
Stanford University
Stanford, California USA 94305

ABSTRACT

The transverse eigenmodes of optical resonators are not in general orthogonal to each other, but rather are biorthogonal to an adjoint set of functions which turn out to be the transverse eigenmodes for propagation in the reverse direction around the same resonator. We present a fairly general derivation of this property which is valid for ring or standing-wave and for stable or unstable resonators with arbitrary output mirror profiles. We also point out certain unusual consequences of these properties for high-magnification unstable resonators.

ORTHOGONALITY PROPERTIES OF OPTICAL RESONATOR EIGENMODES

by

A. E. Siegman

Edward L. Ginzton Laboratory
Stanford University
Stanford, California USA 94305

I. INTRODUCTION

The orthogonality properties of optical resonator transverse modes appear to be, if not inadequately understood, at least not very widely understood and very little discussed in the literature [1-3]. The basic operators that determine optical resonator transverse eigenmodes are in general not hermitian, and therefore these eigenmodes are not in general orthogonal in the (u^*, u) sense, where u^* means complex conjugate. Consider first a simple two-mirror standing-wave resonator with arbitrarily shaped but uniformly reflecting mirror surfaces. The Huygens kernel for the standard "Fox-and-Li" approach to finding the resonator eigenmodes is then symmetric between points on the mirror surfaces. The resonator eigenmodes in this case are therefore orthogonal in the (u, u) sense over the mirror surfaces [3]. The fundamental adjoint properties of the wave equation and its associated Green's function [4] strongly indicate that this orthogonality property probably applies much more generally to a broader class of resonators.

Arnaud [5] discusses the biorthogonal eigenmodes of general complex-paraxial resonators, stable or unstable, having general hermite-gaussian modes. He points out that there is a set of adjoint eigenmodes u^\dagger which are biorthogonal to the usual set of resonator eigenmodes u in this case, and that the adjoint modes are physically the transverse eigenmodes for propagation in the reverse direction around the same resonator. Again it seems likely that this result applies more generally to nearly all optical resonators.

The purpose of this note is to present a simple derivation which demonstrates the biorthogonality properties of the eigenmodes of an optical resonator under still more general conditions, including an arbitrary output mirror profile in both phase and amplitude. The conclusions obtained then apply to stable and unstable resonators, to ring and standing-wave resonators, and especially to resonators with non-paraxial and non-uniform elements located at least one plane within the cavity. We also note that these biorthogonality properties imply certain unusual consequences for high-magnification unstable resonators.

APPENDIX VI

RESONANT MODES OF OPTICAL CAVITIES
WITH PHASE-CONJUGATE MIRRORS

Pierre A. Bélanger,^{*} Amos Hardy,^{**} and A. E. Siegman

Edward L. Ginzton Laboratory
Department of Electrical Engineering
Stanford University
Stanford, California 94305

(Revised 25 October 1979)

ABSTRACT

We derive the lowest-order self-consistent gaussian transverse modes and also the resonant frequencies of an optical resonator formed by conventional paraxial optical components plus a phase-conjugate mirror (PCM) on one end. The conventional optical elements are described by an overall ABCD matrix. Cavities with purely real elements (no aperturing) have a continuous set of self-reproducing gaussian modes, described by a semicircular locus in the $1/q$ plane for one round trip; all gaussian beams are self-reproducing after two round trips. Complex ABCD matrices, such as are produced by gaussian aperturing in the cavity, lead to unique self-consistent perturbation-stable gaussian modes. The resonant frequency spectrum

^{*} On leave from Laval University, Quebec, Canada.

^{**} On leave from the Weizmann Institute of Science, Isreal.

of a PCM cavity consists of a central resonance at the driving frequency ω_0 of the PCM element, independent of the cavity length L , plus "half-axial" sidebands spaced by $\Delta\omega_{ax} = 2\pi(c/4L)$, with phase and amplitude constraints on each pair of upper and lower sidebands.

Pierre Bélanger is on leave from Laval University, Quebec, Canada, on leave to Stanford University. Amos Hardy is a Chaim Weizmann Fellow on leave from the Weizmann Institute of Science, Israel, on leave to Stanford University. Anthony E. Siegman is with the Edward L. Ginzton Laboratory and Department of Electrical Engineering, Stanford University, Stanford, California 94305.

Received

I. INTRODUCTION

The emerging subject of phase conjugate optics is receiving much attention at present.^{1,2,3} The basic building block for phase conjugate optics is the phase conjugate mirror (PCM), an optical element that has the unusual property of converting an incident optical wave into a reflected wave whose complex phasor amplitude is the complex conjugate of the incident wave. In practice phase-conjugate reflection is most often accomplished by means of four-wave mixing in a nonlinear optical medium, such as an optical Kerr cell, when this medium is actively pumped by two coherently related, counter-propagating pump beams. Phase-conjugate reflection can also be accomplished using three-wave mixing (degenerate parametric mixing) but with severe practical limitations set by phase-matching requirements.

Since the phase conjugate mirror is an interesting and unusual new component, our objective in this paper is to explore the transverse and longitudinal resonant mode properties of optical cavities having phase conjugate mirrors as one of their end reflectors. To our knowledge only one laser has yet been operated using such a pure PCM end mirror.⁴ Several other analyses of this topic have appeared while this paper was in preparation.^{4,5,6} Our results here partially overlap and partially complement and extend these contributions.

In this paper we first carry out in Section II a general derivation of the lowest-order gaussian transverse mode properties of a PCM laser cavity.

We include the possibility of radially varying transmission or gain, which leads to complex-valued paraxial elements. Section III then explores a few specific examples of the transverse modes in simple PCM cavities containing either gaussian apertures (i.e., thin elements with gaussian radial apodization) or gaussian ducts (i.e., thick elements with gaussianly varying transmission). Finally in Section IV we discuss the somewhat unusual resonant-frequency or axial-mode characteristics, particularly the existence of "half-axial" modes, that are characteristic of PCM laser cavities.

II. GAUSSIAN TRANSVERSE MODE ANALYSIS

A. Round-Trip Gaussian Beam Propagation

We consider as our basic model an ideal PCM reflector placed at one end of a general multi-element optical resonator, as in Fig. 1. A PCM reflector has the basic property that if the optical wave incident on the reflector along the positive z axis has the form at any reference plane z

$$E_{inc}(x,y,z,t) = \text{Re } \tilde{E}(x,y,t) e^{j(\omega_0 t - kz)} \quad (1)$$

where x,y are transverse coordinates across a reference plane, then the reflected wave at the same plane has the form

$$E_{refl}(x,y,z,t) = \text{Re } \tilde{\kappa} \tilde{E}^*(x,y,t) e^{j(\omega_0 t + kz)} \quad (2)$$

where $\tilde{\kappa}$ is a PCM reflection coefficient which may be complex (i.e., have a phase angle). The frequency ω_0 is the reference optical frequency given by the frequency of the pump lasers necessary to drive the nonlinear medium used in the PCM.

As a consequence of the phase conjugation, a gaussian optical beam bouncing off a PCM will have its radius of curvature R reversed in sign, but its spot size w unchanged (except for a potential generalization to be discussed

later). If we define the complex q parameter for a gaussian beam in the usual way, i.e.

$$\frac{1}{q} \equiv \frac{1}{R} - j \frac{\lambda}{\pi w^2} \quad (3)$$

then the reflective property of the PCM in Fig. 1 can be expressed mathematically by

$$q_2 = -q_1^* \quad (4)$$

The other optical elements in the resonator outside of the PCM can be described by a general paraxial, possibly complex-valued ABCD matrix which sums up a complete round-trip from the reference plane out through the resonator and back to the PCM. Since this is an "out-and-back" journey, the ABCD matrix has the general property that $A = D$. We assume negligible diffraction effects at any apertures or stops inside the resonator.

A gaussian beam with a general complex gaussian beam parameter q_2 when it leaves the PCM will then return with a gaussian parameter q_1' given by

$$q_1' = \frac{Aq_2 + B}{Cq_2 + D} \quad (5)$$

Therefore a complete round trip around the entire PCM cavity may be expressed by the net transformation

$$\frac{B}{q_1'} = \frac{\Lambda^2 - 1 - \Lambda B/q_1^*}{A - B/q_1^*} \quad (6)$$

where we have used the fact that the paraxial ray matrix will obey the relationship $AD - BC = 1$.

The self-consistent or self-reproducing solutions to Eq. (6), defined by the condition that $q_1' = q_1 = q$, are then given by the solutions to

$$\frac{B^2}{qq^*} - AB \left(\frac{1}{q} + \frac{1}{q^*} \right) + A^2 - 1 = 0 \quad (7)$$

This defines either a circular locus or a unique singular point in the $1/q$ plane, depending only on whether the ABCD coefficients are purely real or complex.

B. Real Paraxial Systems

For purely real ABCD elements Eq. (7) is a purely real equation, which may be recast into the useful form

$$\left(\frac{B\lambda}{\pi w^2} \right)^2 + \left(\frac{B}{R} - A \right)^2 = 1 \quad (8)$$

This defines a displaced unit circle in the complex B/q plane, that is, in a plane with rectangular coordinate axes $x \equiv B/R$ and $y \equiv B\lambda/\pi w^2$, as shown in Fig. 2(a). This displaced unit circle has radius unity and center at $B/R = A$, $B\lambda/\pi w^2 = 0$. There is evidently no unique self-consistent transverse mode for the PCM cavity with purely real elements. Any gaussian beam corresponding to a point on the semicircular locus represents an equally valid self-consistent confined mode.

Physical insight into this situation can be obtained by examining the variation of an arbitrary gaussian beam on two successive round trips, starting from any arbitrary q value determined by an initial R and w , located for example inside the self-consistent locus. The complex vector $(B/q - A)$ from the center of the circle $(A, 0)$ to the initial point B/q in the complex plane, and the corresponding vector $(B/q' - A)$ after one round trip are then related by

$$(B/q - A)(B/q' - A)^* = 1 \quad (9)$$

This describes geometrically an inversion with respect to the displaced unit circle in the complex B/q plane, as illustrated in Fig. 2(b). This necessarily implies that a second round trip will reinvert the q' parameter back to its original q starting place. Hence, with real ABCD elements all gaussian beams are self-reproducing after two round trips. The parameter q (or B/q) bounces back and forth between conjugate points inside and outside the self-consistent locus, as illustrated in Fig. 2(b).

This behavior occurs because the PCM acts in essence as an automatically adjusting lens which exactly refocuses a wave so as to simply change the sign of R . Figure 3 shows an unfolded model for a PCM cavity, illustrating the automatic self-consistency after two round trips.

We may also conclude that the confined self-consistent solution at any point on the displaced semicircle is marginally stable - which means it is effectively stable - against perturbations in the sense introduced by Casperson.⁷ This occurs because any input beam that is displaced very

slightly from any point on the self-consistent locus will bounce back and forth across the locus, without any growth of the displacement.

The type of self-consistent mode analysis we have carried out here using a reference plane in front of the PCM can, alternatively, be carried out using a reference plane located on the opposite end mirror surface of the cavity, e.g. on the left-hand mirror surface in a cavity like Fig. 1. The result of such an analysis shows that, for real ABCD elements, the phase front of the gaussian beam exactly matches the mirror surface (the wave radius R coincides with the mirror radius of curvature); while the spot size w on the mirror surface is arbitrary. This property of PCM resonator modes was pointed out earlier by AuYeung.⁴ The locus of q values, referenced to the end mirror surface, is thus a vertical line in the $1/q$ plane of Fig. 2. The one-way propagation from this mirror through the optical elements to the PCM end of the cavity is a biorthogonal transformation in the $1/q$ plane which converts this vertical line into the circular locus of Fig. 2 as the spot size on the end mirror surface varies.

The allowed values of the gaussian-beam q parameter are thus distributed along a continuous locus for real ABCD values, rather than being limited to a single point. However, it seems very likely both from conclusions we will derive in the following section and from the analysis of Bel'dyugin, Galushkin, and Zanskov,⁶ that if any kind of weak aperture is added inside the PCM cavity, diffraction effects will remove this degeneracy. The cavity will then converge to a unique quasi-gaussian mode near that point on the semicircular locus which minimizes the diffraction losses at the aperture.

C. Complex Paraxial Systems

In the most general paraxial case an optical cavity may include among its elements a "gaussian aperture", by which we mean a thin apodized element with a radial amplitude transmission varying as $\exp(-\alpha x^2)$, and/or a "gaussian duct", by which we mean a thick element with the same property. Such elements can be described as complex paraxial elements - that is, all of the rules of paraxial optics with ABCD matrices remain valid, but at least some and potentially all of the ABCD matrix elements become complex-valued quantities.

It becomes convenient in this case to write the ABCD matrix elements in the general form

$$\begin{aligned} A &= A_0 e^{j\theta_A} \\ B &= B_0 e^{j\theta_B} \end{aligned} \tag{10}$$

where A_0 and B_0 are the absolute magnitudes of the complex elements A and B . The angles θ_A and θ_B in general have finite values determined by the gaussian variable amplitude transmission elements inside the optical system. These angles go either to 0 or to π as the strength of the gaussian aperturing goes to zero (the value π meaning that the matrix element becomes real but negative).

We note here that a gaussian transverse variation of the amplitude transmission may be produced by the PCM mirror itself. That is, the 4-wave mixing cell used to produce the PCM may be pumped by pump beams which have gaussian transverse amplitude variations; and this in turn will produce a gaussian transverse variation in the magnitude of the PCM reflection coefficient $\tilde{\kappa}$. The net effect will be the same as if a gaussian aperture were added to the optical system just in front of the PCM. ⁸

The self-consistency equation (7) now becomes complex, with finite real and imaginary parts. These yield, after a little algebra, the unique self-consistent solutions

$$\frac{B_0}{R_{sc}} = A_0 \cos(\theta_B - \theta_A) - \frac{\sin 2\theta_B}{2A_0 \sin(\theta_B - \theta_A)} \quad (11)$$

and

$$\left(\frac{B_0 \lambda}{\pi w_{sc}^2}\right)^2 = \frac{[A_0^2 \sin^2(\theta_B - \theta_A) - \sin^2 \theta_B][A_0^2 \sin^2(\theta_B - \theta_A) + \cos^2 \theta_B]}{A_0^2 \sin^2(\theta_B - \theta_A)} \quad (12)$$

$$= \cos 2\theta_B + A_0^2 \sin^2(\theta_B - \theta_A) - \left(\frac{\sin 2\theta_B}{2A_0 \sin(\theta_B - \theta_A)}\right)^2$$

These results say that if the condition is satisfied that

$$\sin^2 (\theta_B - \theta_A) \geq \frac{\sin^2 \theta_B}{A_0^2} \quad (13)$$

then a complex-valued paraxial system will have a unique, confined ($w^2 > 0$), self-consistent, lowest-order gaussian mode, corresponding to a point, not a curve, in the B/q plane. As θ_A and θ_B approach zero, this point approaches in the limit a location somewhere on the semicircular locus for real ABCD systems. However, just where this limiting point falls on the displaced unit circle locus depends on A_0 and on the relative values of the angles θ_A and θ_B , as we will illustrate in the following section.

Suppose in particular that θ_A and θ_B are both small, approaching zero in the limit. Then the self-consistent solution is

$$\frac{B}{R_{sc}} \approx A_0 - \frac{\theta_B}{A_0(\theta_B - \theta_A)} \quad (14)$$

$$\left(\frac{B_0 \lambda}{\pi w_{sc}^2} \right)^2 \approx 1 - \left(\frac{\theta_B}{A_0(\theta_B - \theta_A)} \right)^2$$

To this level of approximation the complex self-consistent point lies on the displaced unit circle, at an angle φ from the x axis given by

$$\cos \varphi \approx \frac{-\theta_B}{A_0(\theta_B - \theta_A)} \quad (15)$$

as illustrated in Fig. 4.

We must also check whether the complex self-consistent solution given by (11) and (12) is perturbation-stable in the sense described by Casperson.⁷

If a gaussian beam starts around the PCM cavity with an initial gaussian beam parameter given by $q_{sc} + \Delta q$, where q_{sc} is the self-consistent value given by (11) and (12), and Δq is a small complex perturbation, then after one round trip the beam will be described by $q_{sc} + \Delta q'$ where $\Delta q'$ is a slightly different perturbation. Perturbation stability requires that $|\Delta q'/\Delta q| \leq 1$. For the PCM resonator it can be shown that after one round trip

$$\begin{aligned} \left| \frac{\Delta q'}{\Delta q} \right|^2 &= \frac{[\operatorname{Re}(A/B - 1/q_{sc})]^2 + [\operatorname{Im}(A/B - 1/q_{sc})]^2}{[\operatorname{Re}(A/B - 1/q_{sc})]^2 + [\operatorname{Im}(A/B + 1/q_{sc})]^2} \\ &= \frac{[A_0 \cos(\theta_B - \theta_A) - B_0/R_{sc}]^2 + [A_0 \sin(\theta_B - \theta_A) - B_0\lambda/\pi w_{sc}^2]^2}{[A_0 \cos(\theta_B - \theta_A) - B_0/R_{sc}]^2 + [A_0 \sin(\theta_B - \theta_A) + B_0\lambda/\pi w_{sc}^2]^2} \end{aligned} \quad (16)$$

This is less than or equal to unity if

$$\operatorname{Im}(A/B) \leq 0 \quad (17)$$

or

$$\sin(\theta_B - \theta_A) \geq 0 \quad (18)$$

Figure 4 illustrates how a stable system, starting from an arbitrary initial q value, will converge in to the self-consistent value q_{sc} upon repeated bounces.

III. EXAMPLES OF COMPLEX PCM RESONATORS

A. Plane-Mirror Cavity With Gaussian Aperture

As a particular example of a complex PCM resonator let us consider a cavity consisting of a plane mirror and a PCM separated by distance L , plus a gaussian aperture with amplitude transmission $T(r) = \exp(-r^2/a^2)$ located at a distance L_a from the plane mirror, as in Fig. 5(a). We may define an aperture strength parameter F and a normalized aperture location X by

$$F \equiv \frac{\pi a^2}{L\lambda}, \quad X \equiv \frac{L_a}{L} \quad (19)$$

The complex paraxial matrix elements are then given by

$$\begin{aligned} A &= 1 - 2X(1 - X)/F^2 - j 2/F \\ B &= 2L [1 - X(1 - X)^2/F^2 - j (1 - X^2)/F] \end{aligned} \quad (20)$$

In the limit of weak aperturing ($F \rightarrow \infty$) this gives

$$\begin{aligned} A_o &\approx 1, \quad B_o \approx 2L \\ \theta_a &\approx -2/F, \quad \theta_B \approx -(1 - X^2)/F \end{aligned} \quad (21)$$

The self-consistent solutions at a reference plane just inside the PCM are

$$\frac{L}{R_{sc}} \approx \frac{1}{1 + X^2}$$

$$\frac{L\lambda}{\pi w_{sc}^2} \approx \frac{X}{1 + X^2}$$
(22)

These solutions move along a contour in the $1/q$ plane as in Fig. 5(b). As the gaussian aperture moves close to the plane mirror ($X \rightarrow 0$) the self-consistent mode approaches a spherical wave centered on the plane mirror, with zero spot size at the aperture and infinite spot size at the PCM, as in Fig. 5(c). In the opposite limit as the gaussian aperture moves close to the PCM ($X \rightarrow 1$) the mode becomes essentially a half-confocal resonator mode, with a minimum spot size $w = (2L\lambda/\pi)^{1/2}$ at the PCM end as in Fig. 5(d).

B. Plane-Mirror Cavity With Gaussian Aperture and Gaussian Duct

Consider next a plane-mirror cavity of length L having a gaussian aperture located immediately in front of (or possibly inside) the PCM, but with the remainder of the cavity also filled with a gaussian duct, or a transversely varying gain medium, as in Fig. 6(a). The propagation constant k in this medium is assumed to have a complex radial variation given by

$$k^2(r) = k_0^2 [1 - j\eta r^2]$$
(23)

The case $\eta > 0$ corresponds to a radially increasing loss in the medium, or alternatively to a gain medium with a maximum gain on axis and radially decreasing gain off axis. Alternatively $\eta < 0$ corresponds to an "anti-duct" with a gain minimum (or loss maximum) on axis.

If we use the same definition $F = \pi a^2 / L\lambda$ as above for the gaussian aperture, then the matrix elements are

$$\begin{aligned} A &= 1 - 2j (1/F + \eta L^2) \\ B &= 2L (1 - 2j\eta L^2/3) \end{aligned} \tag{24}$$

In the limit of a weak gaussian aperture ($|F| \rightarrow \infty$) and weak gaussian ducting ($|\eta| \rightarrow 0$) the self-consistent solutions are

$$\begin{aligned} \frac{2L}{R_{sc}} &= 1 + \left(\frac{Y}{3 + 2Y} \right) \\ \left(\frac{2L\lambda}{\pi w_{sc}^2} \right)^2 &= 1 - \left(\frac{Y}{3 + 2Y} \right)^2 \end{aligned} \tag{25}$$

where Y is the parameter

$$Y \equiv F\eta L^2 \tag{26}$$

As $|F| \rightarrow \infty$ and $|\eta| \rightarrow 0$, the parameter Y can take on any value in the range $-\infty \leq Y \leq \infty$ depending on the relative magnitudes of F and η .

That is to say, Y is a measure of the relative strengths of the gaussian aperture and the gaussian duct even when both become very weak.

A confined self-consistent gaussian mode only exists for values of Y within the ranges

$$Y \equiv F\eta L^2 \geq -1 \quad (27)$$

or

$$Y \equiv F\eta L^2 \leq -3 \quad (28)$$

These ranges define a complete semicircle in the $1/q$ plane, as illustrated in Fig. 6. However the perturbation stability criterion of Eq. (18) is satisfied only for

$$\left(\frac{1}{F} + \frac{2\eta L^2}{3} \right) \geq 0 \quad (29)$$

For $F > 0$, which means a positive or converging gaussian aperture, the overall system can still be stable even if the gaussian duct becomes an "anti-duct" with radially increasing transmission, but this holds only over the limited range $Y = F\eta L^2 \geq -2/3$. Alternatively for $F < 0$, which would mean a negative or diverging gaussian aperture, the gaussian duct must have a transmission maximum on axis of relative strength sufficient to make $Y = F\eta L^2 \geq +2/3$. Figure 6(b) uses dashed lines to indicate the portions of the self-consistent locus that represent confined but not perturbation-stable solutions for the case $F > 0$. This example rather clearly

illustrates how a mixture of positive and negative gaussian aperturing can lead to such confined but perturbation-unstable modes.

C. General Cavity With Gaussian Aperture

As a final example we consider a PCM resonator with a gaussian aperture immediately in front of the PCM and an arbitrary real ABCD system outside this. The complex ABCD values then become

$$\begin{aligned} A &= A_r - j \frac{\lambda B_r}{\pi a^2} \\ B &= B_r \end{aligned} \tag{30}$$

where A_r and B_r are the purely real values. The self-consistent solution then becomes

$$\begin{aligned} \frac{B_r}{R_{sc}} &= A_r \\ \left(\frac{B_r \lambda}{\pi w_{sc}^2} \right)^2 &= 1 + \left(\frac{B_r \lambda}{\pi a^2} \right)^2 \end{aligned} \tag{31}$$

For an arbitrarily weak gaussian aperture ($\lambda/\pi a^2 \rightarrow 0$) the self-consistent value approaches in the limit the point at the top of the semicircle in the B/q plane. No matter how weak the aperture, the mode still attempts to minimize the spot size w_{sc} at the plane of the aperture.

A particular case of interest is a cavity of this type consisting only of a mirror of radius R_0 at distance L from the PCM and the gaussian aperture. The real matrix elements are then

$$\begin{aligned} A_r &= 1 - 2L/R_0 \\ B_r &= 2L(1 - L/R_0) \end{aligned} \tag{32}$$

Figure 7 illustrates the locus of self-consistent solutions for different values of the mirror radius R_0 in the limit of weak aperturing, plotted here in the complex L/q plane, not the complex B/q plane. All of these solutions are stable.

IV. RESONANT FREQUENCIES OF PCM CAVITIES

Our final objective is to explore the resonant frequency behavior and the axial modes of a laser cavity having a PCM reflector at one end.

A. Frequency Dependence of PCM Reflectivity

The resonance properties of an optical cavity with a PCM reflector at one end will depend in the most general case on the phase versus frequency characteristics of the PCM reflector, as well as the remainder of the optical cavity. A signal wave at a detuned frequency $\omega_0 + \Delta\omega$ sent into a PCM consisting of a four-wave mixing cell pumped at frequency ω_0 will be reflected as a conjugate idler wave at the oppositely detuned frequency $\omega_0 - \Delta\omega$. In addition, the amplitude of the reflection coefficient will decrease for off-resonance signals because of unavoidable phase mismatch between the signal, pump and idler frequencies over the finite cell length.⁹ The bandwidth of a PCM reflector by itself, in the weak-coupling limit, can be derived as follows.

Consider a four-wave mixing cell having total interaction length L_c , with the reference plane taken to be at the front (i.e. input) plane of the cell. Let the signal input be an off-resonance unit impulse, that is, an optical pulse with carrier frequency $\omega_a + \Delta\omega$ and duration much shorter than the transit time L_c/c through the cell. As this pulse travels through the four-wave mixing cell in the $+z$ direction and interacts with the assumed cw pump waves, it will shed a continuous "tail" of

constant-amplitude idler waves at frequency $\omega_0 - \Delta\omega$ traveling back in the $-z$ direction through the cell. This idler radiation will in fact continue to emerge back out through the front face of the cell for one full transit time after the signal impulse leaves the cell at the opposite end.

The impulse response of the four-wave cell is thus essentially a square pulse of constant amplitude and time duration $2L_c/c$, extending from $t = 0$ to $t = 2L_c/c$ for a reference plane at the front face of the cell. Shifting the reference plane to the center of the cell makes the impulse response symmetric from $-L_c/c$ to L_c/c . The frequency response of the cell is then the Fourier transform of this time impulse response; and the power reflectivity is the magnitude of this frequency response squared, or

$$R(\omega) = R(\omega_0) \left| \frac{\sin \Delta\omega L_c/c}{\Delta\omega L_c/c} \right|^2 \quad (33)$$

This agrees with the results derived by others⁹ in the weak-coupling limit. The power reflectivity has a maximum value $R(\omega_0)$ on resonance and falls off with the familiar $|(\sin x)/x|^2$ dependence on frequency detuning on either side.

B. PCM Cavity Resonance Condition

The PCM reflector thus has a frequency-dependent reflectivity by itself. However, if the PCM cell length L_c is small compared to the length L of the remainder of the optical cavity, then the central lobe of the PCM frequency response will be broad compared to the optical cavity's axial mode spacing. In addition, if the PCM reference plane is taken at the center of

the four-wave mixing cell, the reflectivity at least for the weak-coupling case will have constant absolute phase versus frequency across the main frequency lobe. We will therefore evaluate the resonance properties of a PCM cavity assuming a flat and constant-phase reflectivity for the PCM reflector. These conditions may or may not be achieved in different experimental situations. However, if the cell length L_c is not short compared to the cavity length L , then the off-resonance axial modes will be so far down on the reflectivity curve of the PCM that they may have little chance of oscillating in competition with the central mode in any case. This latter situation has been analyzed in more detail by AuYeung et al.⁴

The round-trip phase shift of the remainder of the optical cavity will also depend slightly, in second order, on the transverse mode character of the cavity because of the well-known Guoy phase shifts. These effects cause slight transverse-mode shifts for higher order transverse modes, which we are not considering; but otherwise produce in effect only a minuscule change in the effect length of the cavity. We will therefore ignore these and use an essentially transmission-line or plane-wave approach for the main part of the optical cavity.

We therefore adopt a model as shown in Fig. 8, consisting of a four-wave mixing cell located at $z = 0$ and a normal mirror located at $z = -L$ along the z axis. The four-wave mixing cell is pumped by two contradirected waves of complex phasor amplitude \tilde{E}_1 and \tilde{E}_2 at the driving frequency ω_0 . There is also incident on the cell from inside the cavity a signal wave of the general form

$$e(t) = \text{Re } \tilde{E}(t) e^{j\omega_0 t} \quad (34)$$

We now ignore transverse variations (for simplicity) but assume that both the phase and amplitude of the complex phasor $\tilde{E}(t)$ may be time varying in general. We also assume that the absolute phases of all waves are measured at a reference plane located at $z = 0$, in the center of the four-wave-mixing cell. For small incident fields, this will produce a four-wave-reflected or PCM wave given by

$$\mathcal{E}'(t) = \text{Re } \tilde{\kappa} \tilde{E}^*(t) e^{j\omega_0 t} \quad (35)$$

The four-wave-mixing coefficient $\tilde{\kappa}$ (which may in general be complex, with a fixed phase angle) depends on the cell geometry and on the magnitude and phase of the nonlinear susceptibility. It is also directly proportional to the pumping wave phasor amplitudes \tilde{E}_1 and \tilde{E}_2 .

If the round-trip transit time around the cavity from the PCM to the normal mirror and back is $T \equiv 2L/c$, the waves $\mathcal{E}(t)$ and $\mathcal{E}'(t)$ will also be related by

$$\mathcal{E}(t + T) = G^{1/2} \mathcal{E}'(t) \quad (36)$$

where G is the net round-trip power gain due to any laser material (or losses) inside the cavity. For simplicity we assume G has no dispersion. Since we are interested primarily in the resonant frequencies of the cavity we will assume that this round-trip gain and the PCM reflectivity combine to give unity net gain, i.e. $|G^{1/2} \tilde{\kappa}| \equiv 1$. If we denote the net phase angle

of the quantity $\tilde{\kappa}$ by ψ , then from (35) and (36) the round-trip self-consistency condition for the cavity becomes

$$\tilde{E}(t + T) e^{j\omega_0 T} = e^{j\psi} \tilde{E}'(t) = e^{j\psi} \tilde{E}^*(t) \quad (37)$$

Consider first the case when $\tilde{E}(t)$ is constant. If we write the phasor amplitude as

$$\tilde{E} = E_0 e^{j\theta_0} \quad (38)$$

then the self-consistency condition becomes

$$E_0 e^{j(\theta_0 + \omega_0 T)} = E_0 e^{j(\psi - \theta_0)} \quad (39)$$

The cavity has a resonance at ω_0 independent of cavity length L , but the signal at this frequency must have a definite phase θ_0 (measured at $z = 0$) given by

$$2\theta_0 = \psi - \omega_0 T \pmod{2\pi} \quad (40)$$

The waves are in essence not only frequency-synchronized but also phase-synchronized to the frequency ω_0 of the pump waves as modified by the phase angle of $\tilde{\kappa}$.

More generally, suppose that $E(t)$ contains an upshifted signal component at some frequency $\omega_0 + \omega_m$ where ω_m is some as yet unspecified modulation frequency. The phase of $E(t)$ then varies as

$$\tilde{E}(t) \propto e^{j\omega_m t} \quad (41)$$

This will produce a reflected wave

$$\tilde{E}'(t) \propto \tilde{E}^*(t) \propto e^{-j\omega_m t} \quad (42)$$

An upshifted component of $\mathcal{E}(t)$ at $\omega_0 + \omega_m$ thus produces a downshifted component of $\mathcal{E}'(t)$ at $\omega_0 - \omega_m$, which will eventually travel around to become $\mathcal{E}(t)$. We must therefore write $\tilde{E}(t)$ as the combination

$$\tilde{E}(t) = e^{j\theta_0} \left[\tilde{c}_+ e^{j\omega_m t} + \tilde{c}_- e^{-j\omega_m t} \right] \quad (43)$$

where the \tilde{c} 's are complex phasor amplitudes. Putting this into the frequency self-consistency relation (3) and separating like-frequency terms gives

$$\begin{aligned} \tilde{c}_+ &= e^{-j\omega_m T} \tilde{c}_-^* \\ \tilde{c}_- &= e^{j\omega_m T} \tilde{c}_+^* \end{aligned} \quad (44)$$

Combining the first of these relations with the complex conjugate of the second then produces the condition

$$e^{j2\omega_m T} = e^{jn2\pi} \quad (45)$$

where n is any integer. The modulation frequency or sideband frequency ω_m can have any of the values given by

$$\omega_m = n \frac{\pi}{T} = n \cdot 2\pi \left(\frac{c}{4L} \right) \quad (46)$$

These are spaced by half of the usual axial mode spacing for a cavity of length L .

The field $\mathcal{E}(t)$ in the cavity may thus be expanded in resonant modes in the form

$$\begin{aligned} \mathcal{E}(t) &= \tilde{E}(t) e^{j(\omega_0 t + \theta_0)} \\ &= \sum_{n=-\infty}^{\infty} \tilde{c}_n e^{jn(\pi/T)t} e^{j(\omega_0 t + \theta_0)} \end{aligned} \quad (47)$$

with the condition that

$$\tilde{c}_{-n} = (-1)^n \tilde{c}_n^* \quad (48)$$

This is equivalent to writing

$$\begin{aligned} \tilde{E}(t) &= E_0 + j \sum_{n=1,3,\dots} E_n \sin(n\pi t/T + \theta_n) \\ &\quad + \sum_{n=2,4,\dots} E_n \cos(n\pi t/T + \theta_n) \end{aligned} \quad (49)$$

The PCM cavity has a central resonance frequency determined by the pumping frequency ω_0 (not the cavity length L). This central frequency is surrounded by a set of paired "half-axial-mode" resonances spaced by $c/4L$ Hz , or half the usual spacing for a cavity of length L .

This behavior may be understood physically by the following example. Assume that at an initial instant the cavity is entirely filled with radiation at an unshifted frequency $\omega_0 + \Delta\omega$, as in Fig. 9(a) which shows the waves traveling in both directions inside the cavity. The radiation moving toward the PCM will be reflected at the downshifted frequency $\omega_0 - \Delta\omega$, and therefore after a short time the signal inside the cavity will appear as in Fig. 9(b), with lower-frequency radiation now moving away from the PCM. The PCM will continue to take in the higher frequency $\omega_0 + \Delta\omega$ and emit the lower frequency $\omega_0 - \Delta\omega$ until after one complete round-trip time T the cavity will be entirely filled with lower frequency radiation. But, the process will then reverse and the incident signal at $\omega_0 - \Delta\omega$ will be converted back to the original value $\omega_0 + \Delta\omega$. This cycle will be complete after a time $2T$, or two round trips. It is the doubling of the time interval before the signal returns to its original state that leads to the halving of the effective axial mode spacing.

Although the apparent or instantaneous frequency of the cavity signal can oscillate back and forth about the central value ω_0 with period $2T$, amplitude variations will still self-reproduce after period T . Mode locking of this cavity, for example, will produce pulses at intervals of T , not $2T$. However, the apparent frequency of every alternate pulse could oscillate back and forth about ω_0 with period $2T$.

V. CONCLUSIONS

We have carried out the gaussian transverse mode analysis of a resonator formed by conventional paraxial optical components plus a phase conjugate mirror (PCM). For a resonator with only real paraxial elements (no transverse amplitude filtering) any gaussian beam reproduces itself after two round trips; and there is a continuous set of self-consistent q values that reproduce themselves after one round trip. These q values correspond to all possible gaussian beams which match the mirror curvature but have arbitrary spot size, at the opposite end of the cavity from the PCM.

If complex paraxial elements such as gaussian apertures are added to the resonator, there is only one stable self-reproducing or self-consistent gaussian mode of the resonator. Gaussian beams starting from any other point in the $1/q$ plane converge to this self-consistent value upon repeated round trips.

The resonant frequency structure of the PCM cavity contains a central resonance exactly at the PCM pumping frequency ω_0 , independent of the cavity length L . This frequency is surrounded by a set of "half-axial" resonant modes spaced by $c/4L$, or half the usual $c/2L$ axial mode spacing for a cavity of length L . However, there are phase and amplitude constraints on the phasor amplitudes of each pair of sidebands above and below the central frequency.

This work was supported by the U.S. Air Force Office of Scientific Research.

REFERENCES

1. R. W. Hellwarth, "Generation of Time-Reversed Wave Fronts by Nonlinear Refraction," J. Opt. Soc. Am. 67, 1-3 (January 1977).
2. D. M. Bloom and G. C. Bjorklund, "Conjugate Wave-Front Generation and Image Reconstructing by Four-Wave Mixing," Appl. Phys. Lett. 31, 592-594 (1 November 1977).
3. A. Yariv, "Phase Conjugate Optics and Real-Time Holography," IEEE J. Quantum Electron. QE-14, 650-660 (September 1978); see also comments in QE-15, 523-525 (June 1979).
4. J. AuYeung, D. Fekete, D. M. Pepper, and A. Yariv, "Characteristics of Laser Resonators With a Phase Conjugate Mirror," IEEE J. Quant. Electr., in press.
5. J. F. Lam, "Optical Resonators With Phase Conjugate Mirrors," Paper 11, 1 at 1979 IEEE/OSA Conference on Laser Engineering and Applications, Washington, D.C., May 30-June 1, 1979. (Abstract in IEEE J. Quant. Electron. QE-15, 69D (September 1979)).
6. I. M. Bel'dyugin, M. G. Galushkin, and E. M. Zemskov, "Properties of Resonators With Wavefront-Reversing Mirrors," Sov. J. Quant. Electron. 2, 20-23 (January 1979).
7. L. W. Casperson, "Mode Stability of Lasers and Periodic Optical Systems," IEEE J. Quant. Electron. QE-10, 629-634 (September 1974).

8. R. Trebino and A. E. Siegman, "Phase Conjugate Reflection at Arbitrary Angles Using TEM₀₀ Pump Beams," Optics Comm., in press.
9. D. M. Pepper and R. L. Abrams, "Narrow Optical Bandpass Filter Via Nearly Degenerate Four-Wave Mixing," Optics Lett. 3, 212-214 (December 1978).

CAPTIONS FOR FIGURES

1. (a) A typical PCM resonator, and (b) the basic analytical model for discussion of the lowest-order gaussian transverse mode of an optical cavity with a phase-conjugate mirror. The gaussian q parameters are measured at a reference plane immediately in front of the PCM.
2. (a) Locus of self-consistent gaussian beam modes in the $|B|/q$ plane for real ABCD elements. (b) A single round-trip inside the PCM cavity transforms an arbitrary initial point B/q to the geometrically inverted point B/q' with respect to the displaced unit circle. A second round trip returns B/q' to B/q .
3. Unfolded model for two successive round trips in a simple PCM cavity. The PCM acts like a converging lens for a diverging wave (solid lines) but like a diverging lens for a converging wave (dashed lines).
4. A PCM cavity with weak gaussian aperturing has a unique lowest-order self-consistent gaussian mode with a gaussian parameter q_{sc} , corresponding to a single point located on or close to the displaced unit circle. A beam starting from any other initial value of q converges toward the value q_{sc} on repeated bounces.
5. Example of a complex PCM optical cavity containing a plane mirror (PM), gaussian aperture (GA), and phase-conjugate mirror (PCM).

- (a) Cavity model. (b) Self-consistent points in the $1/q$ plane for $X = L_g/L$ ranging from 0 to 1. (c) Self-consistent mode for $X \rightarrow 0$; the spot size approaches zero at one end and infinity at the other. (d) Self-consistent mode for $X \rightarrow 1$; the mode is essentially a half-confocal resonator mode.
6. (a) Optical cavity containing a plane mirror (PM), gaussian duct (GD), gaussian aperture (GA), and phase-conjugate mirror (PCM). (b) Locus of self-consistent solutions in the $1/q$ plane for various values of the relative-strength parameter $Y = F\eta L^2$. Solutions on the solid line are perturbation-stable while those along the dashed regions are confined but perturbation-unstable (for the case $F > 0$).
7. Locus of stable self-consistent solutions for a cavity length L containing a curved mirror of radius R_0 , a weak gaussian aperture, and a phase conjugate mirror, with different values of the parameter R_0/L .
8. Model for analysing the resonant frequencies of a PCM cavity of length L . The PCM cell is pumped at frequency ω_0 and has a reference plane at $z = 0$.
9. (a) A PCM cavity is initially filled with radiation at $\omega_0 + \Delta\omega$. (b) Reflection from the PCM converts the incident radiation at $\omega_0 + \Delta\omega$ to $\omega_0 - \Delta\omega$, as shown here after $\sim 1/4$ of a cavity round trip. (c) After ~ 1 complete round trip, the cavity is now nearly filled with radiation at $\omega_0 - \Delta\omega$, and the reverse process begins.

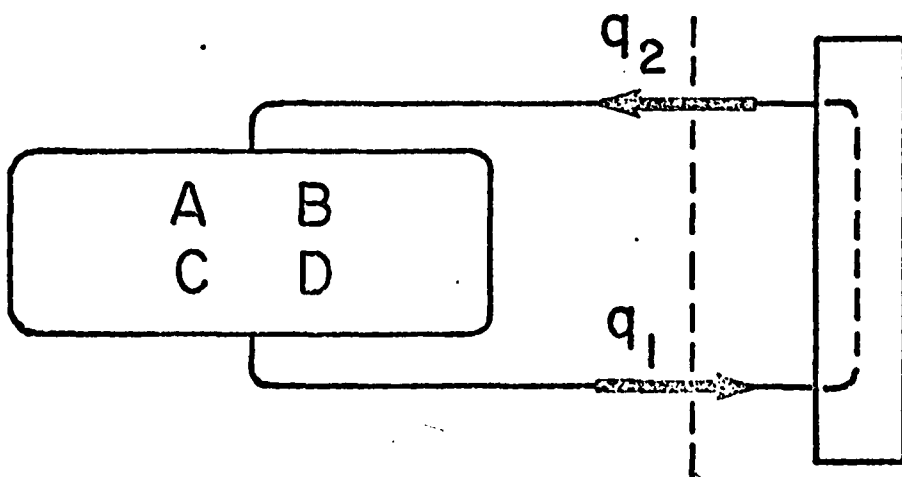
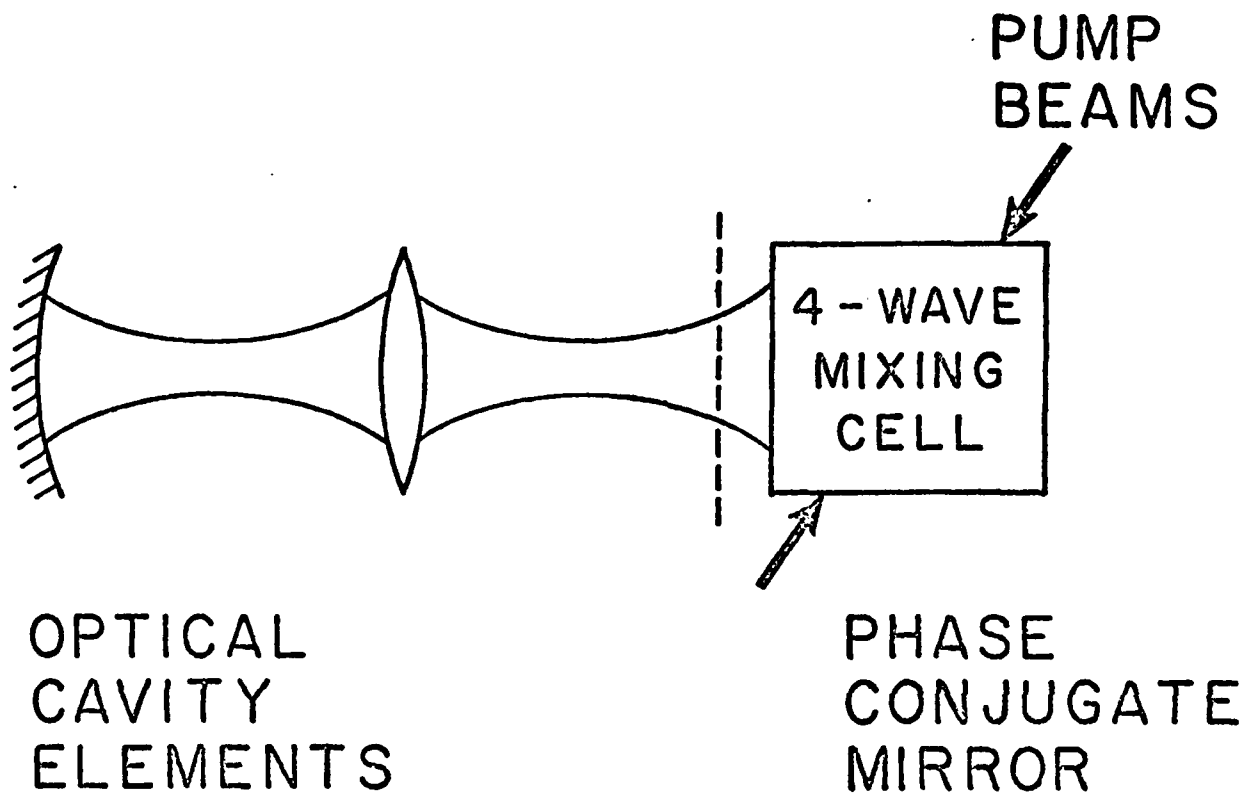
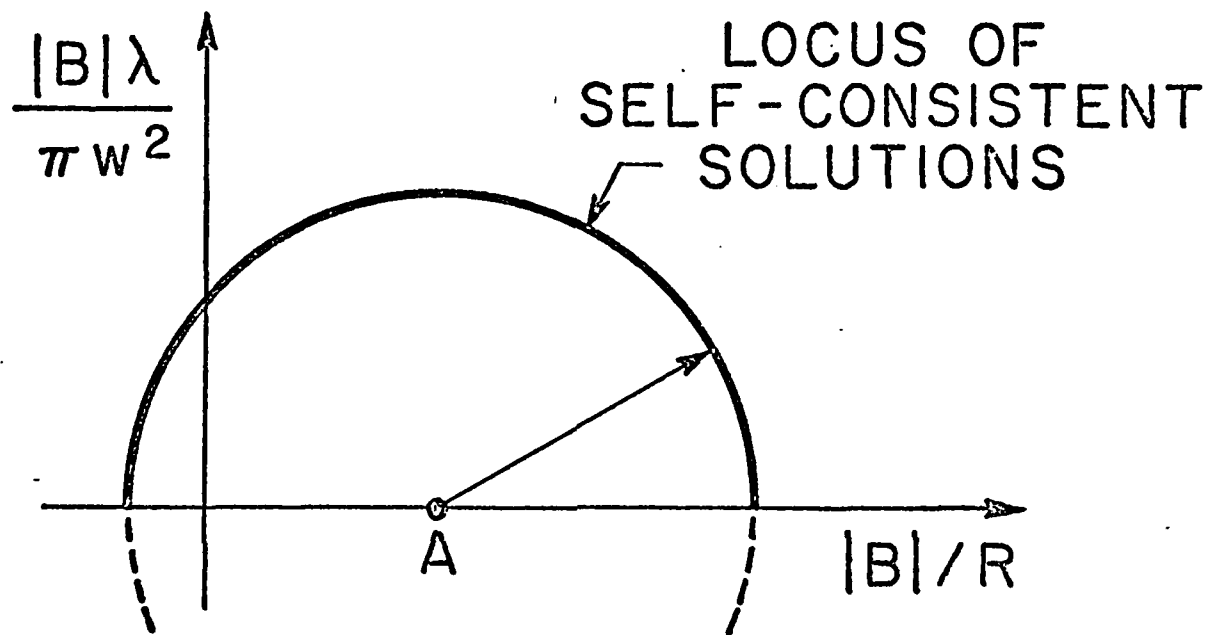
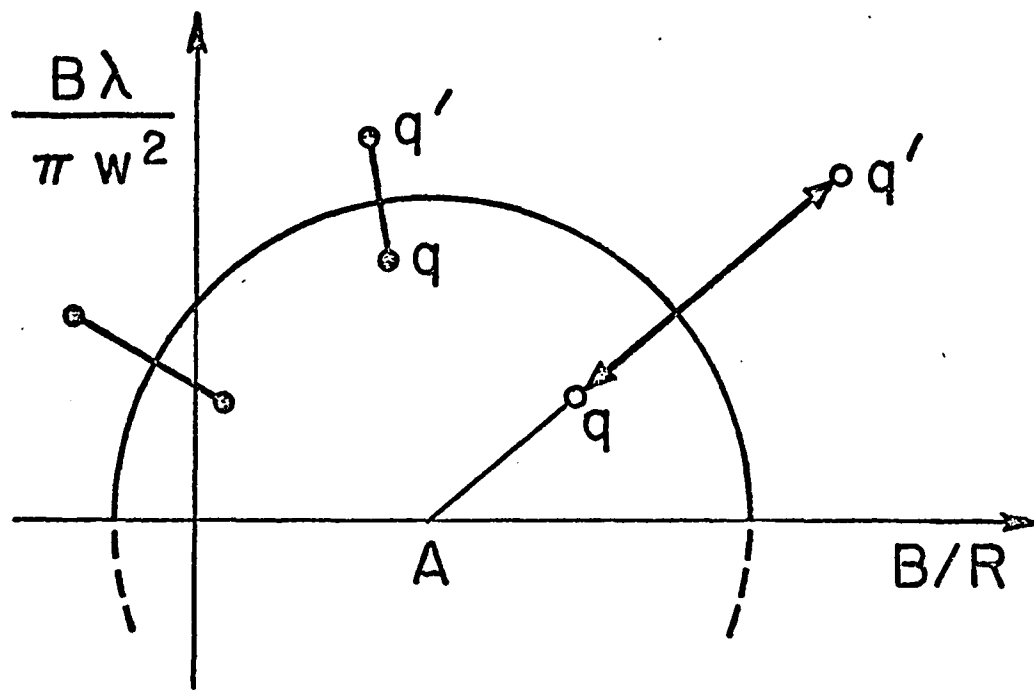


FIGURE 1



(a)

FIGURE 2(a)



(b)

FIGURE 2(b)

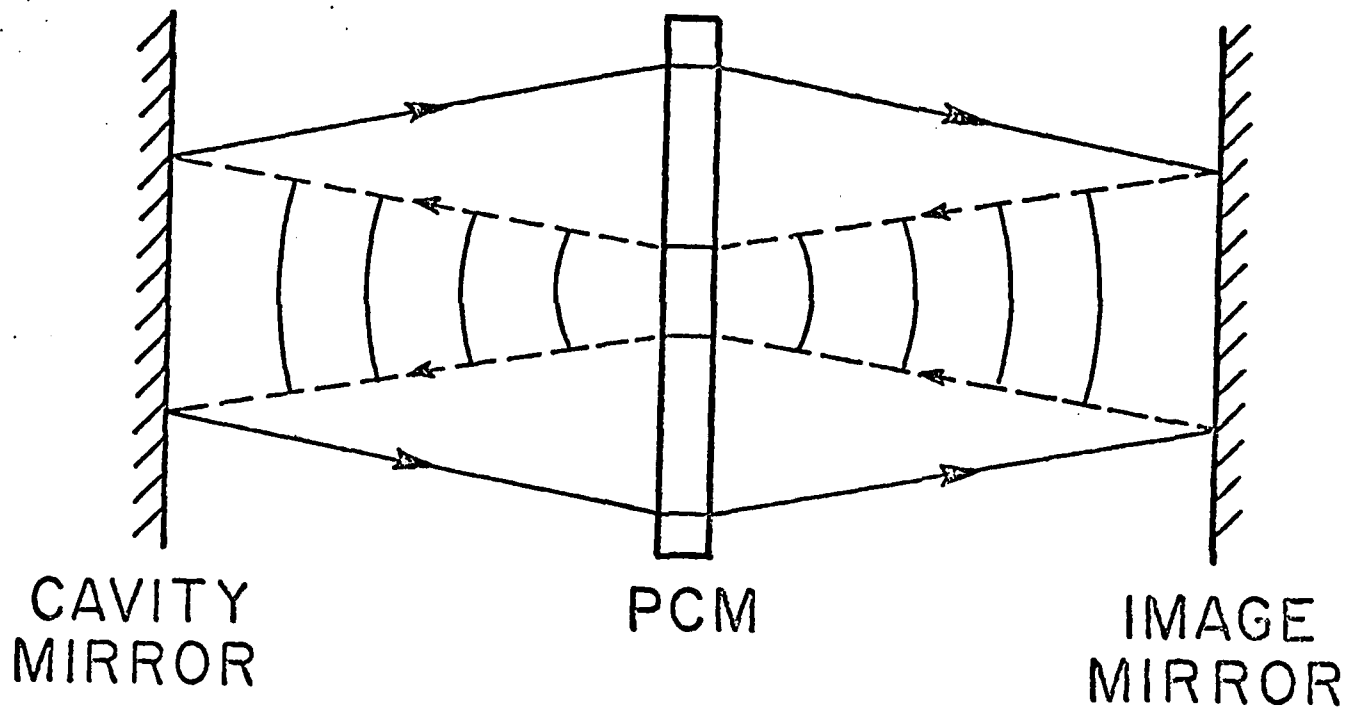


FIGURE 3

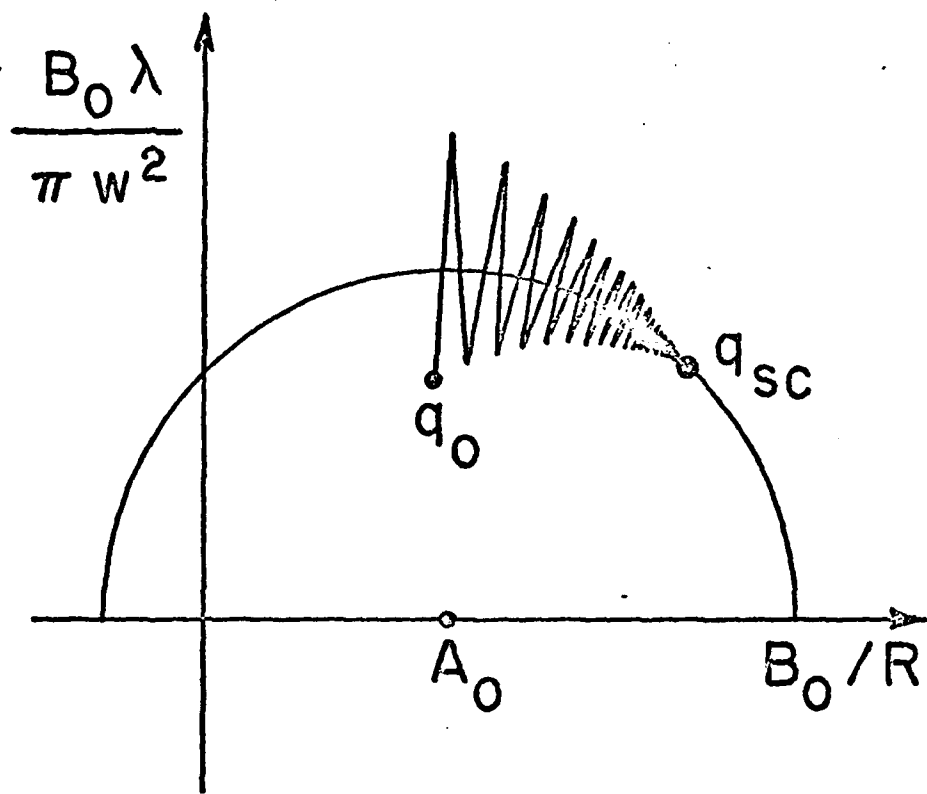
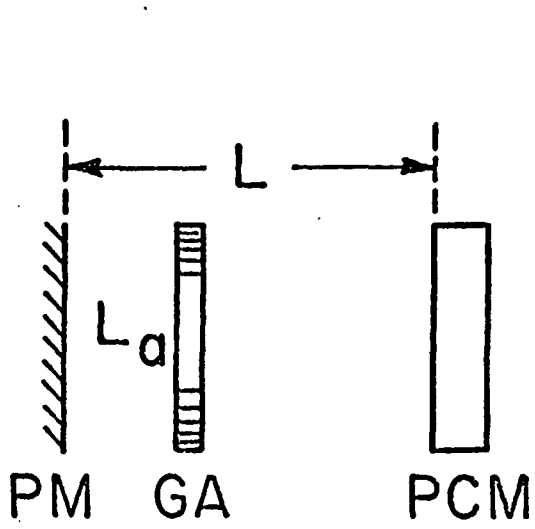
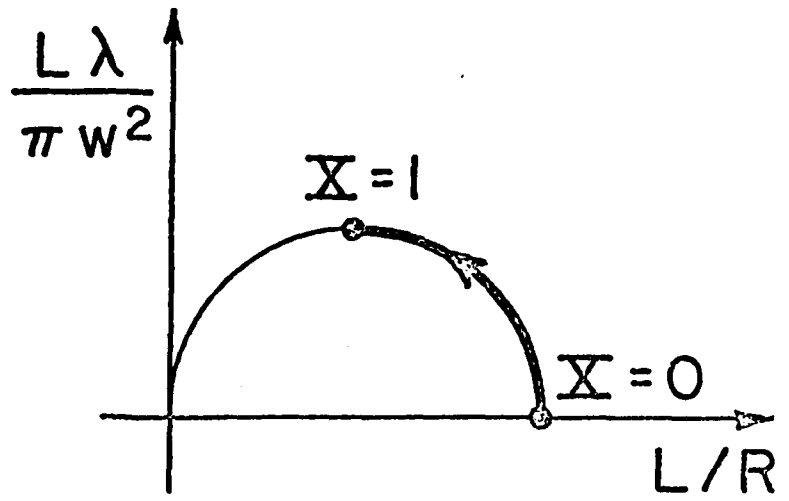


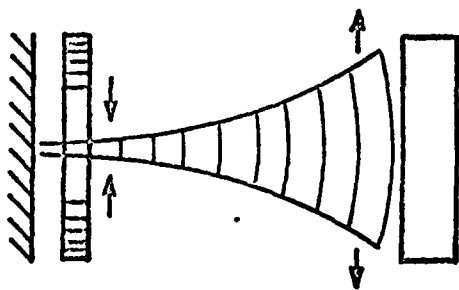
FIGURE 4



(a)

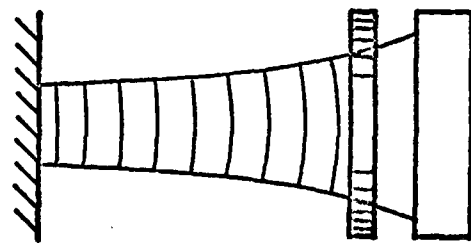


(b)



$X \rightarrow 0$

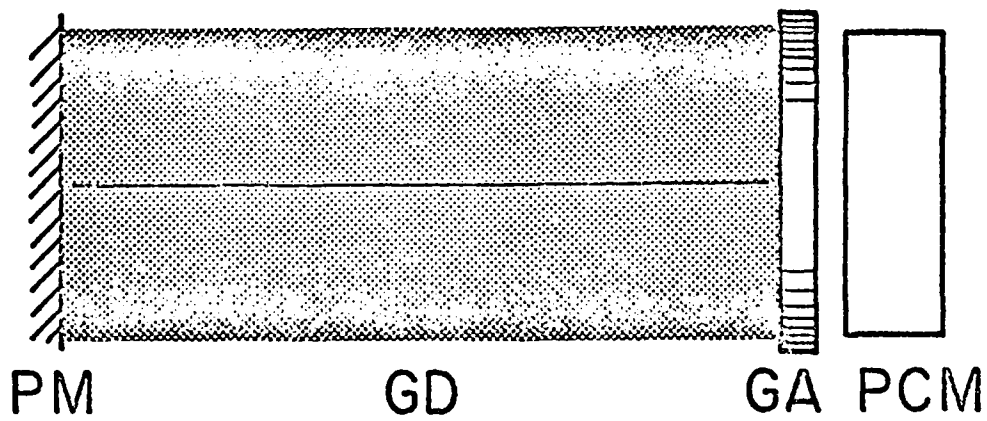
(c)



$X = 1$

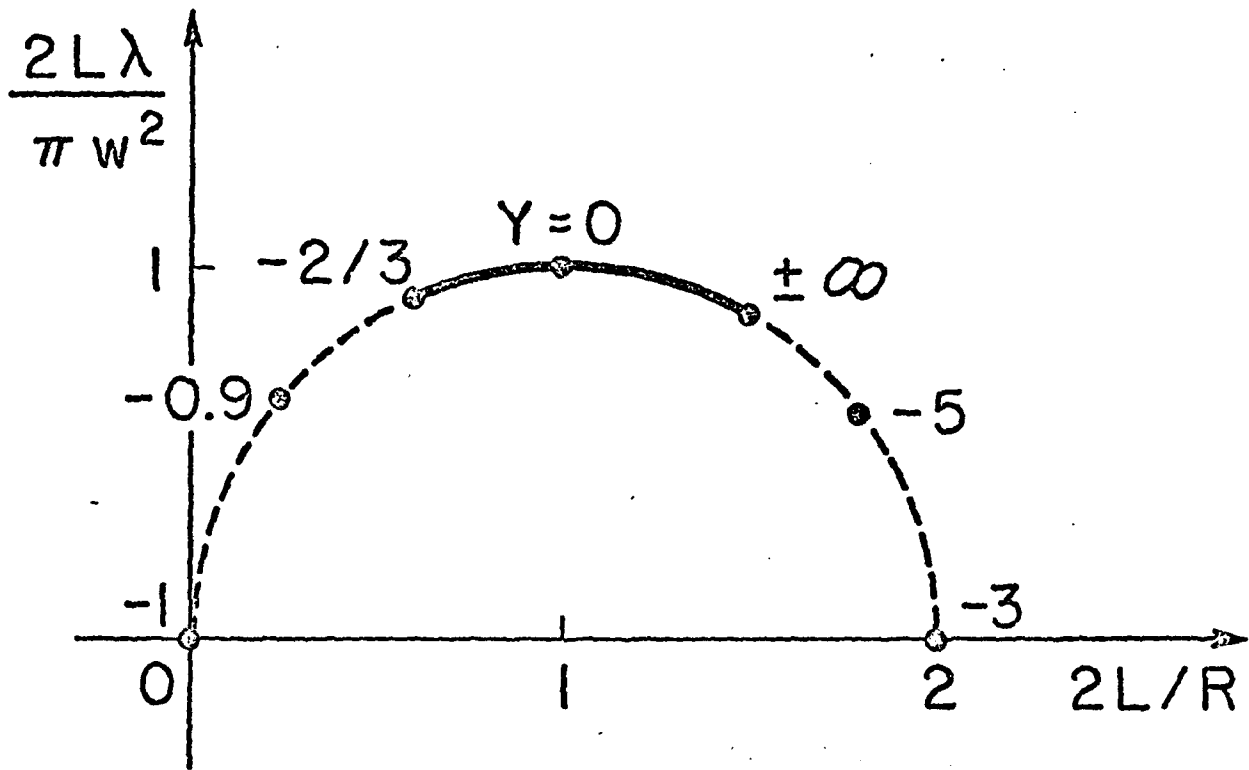
(d)

FIGURE 5



(a)

FIGURE 6(a)



(b)

FIGURE 6(b)

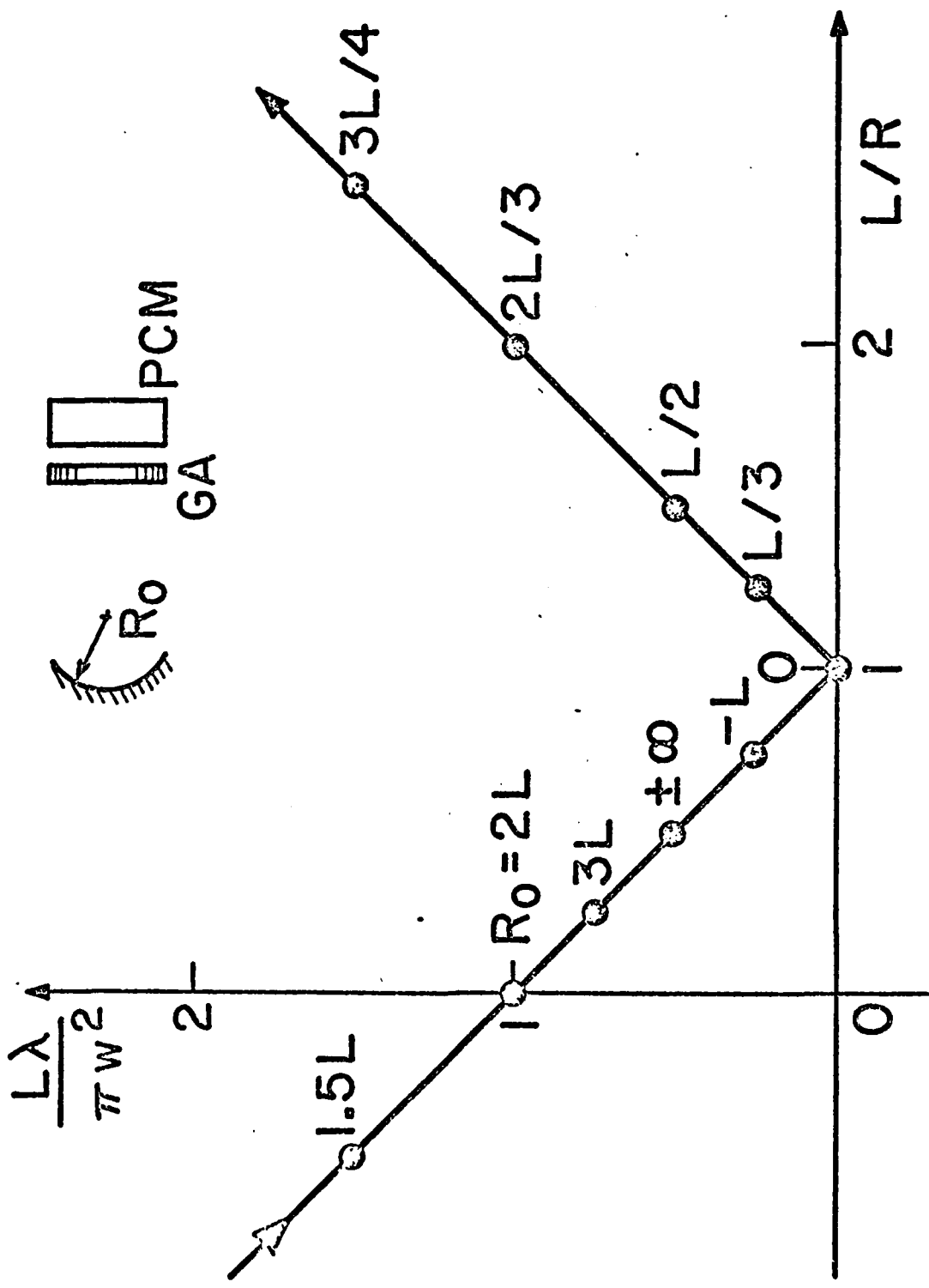


FIGURE 7

AD-A087 245

STANFORD UNIV CA EDWARD L GINZTON LAB
LASER PHYSICS AND LASER TECHNIQUES.(U)
FEB 80 A E SIEGMAN, R L BYER

F/G 20/5

UNCLASSIFIED

GL-3093

F#9620-77-C-0092

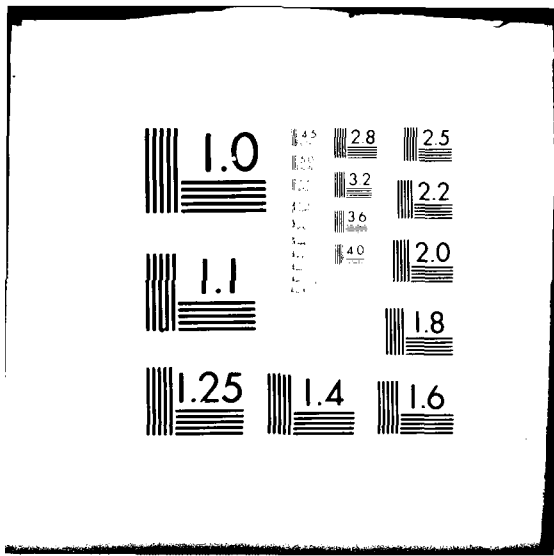
AFOSR-TR-80-0551

NL

2 of 2
AD
A087245



END
DATE
FILMED
9-80
DTIC



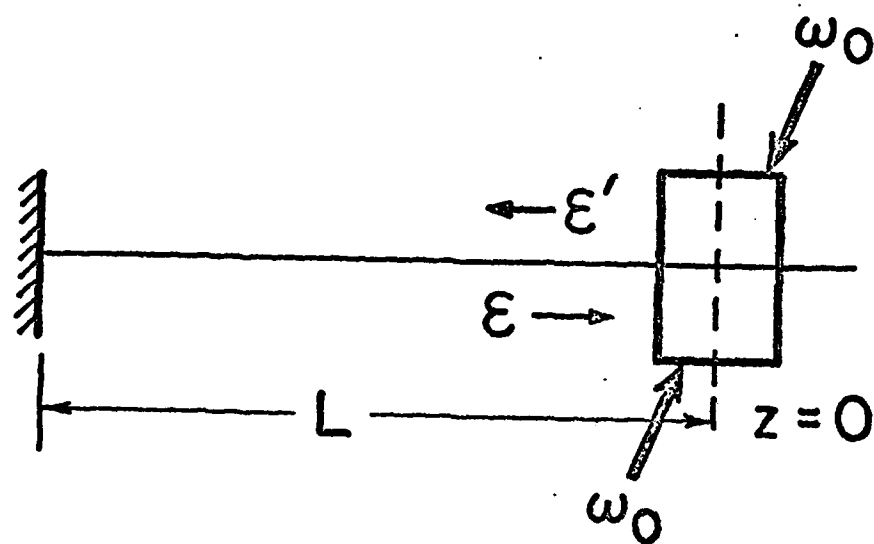


FIGURE 8

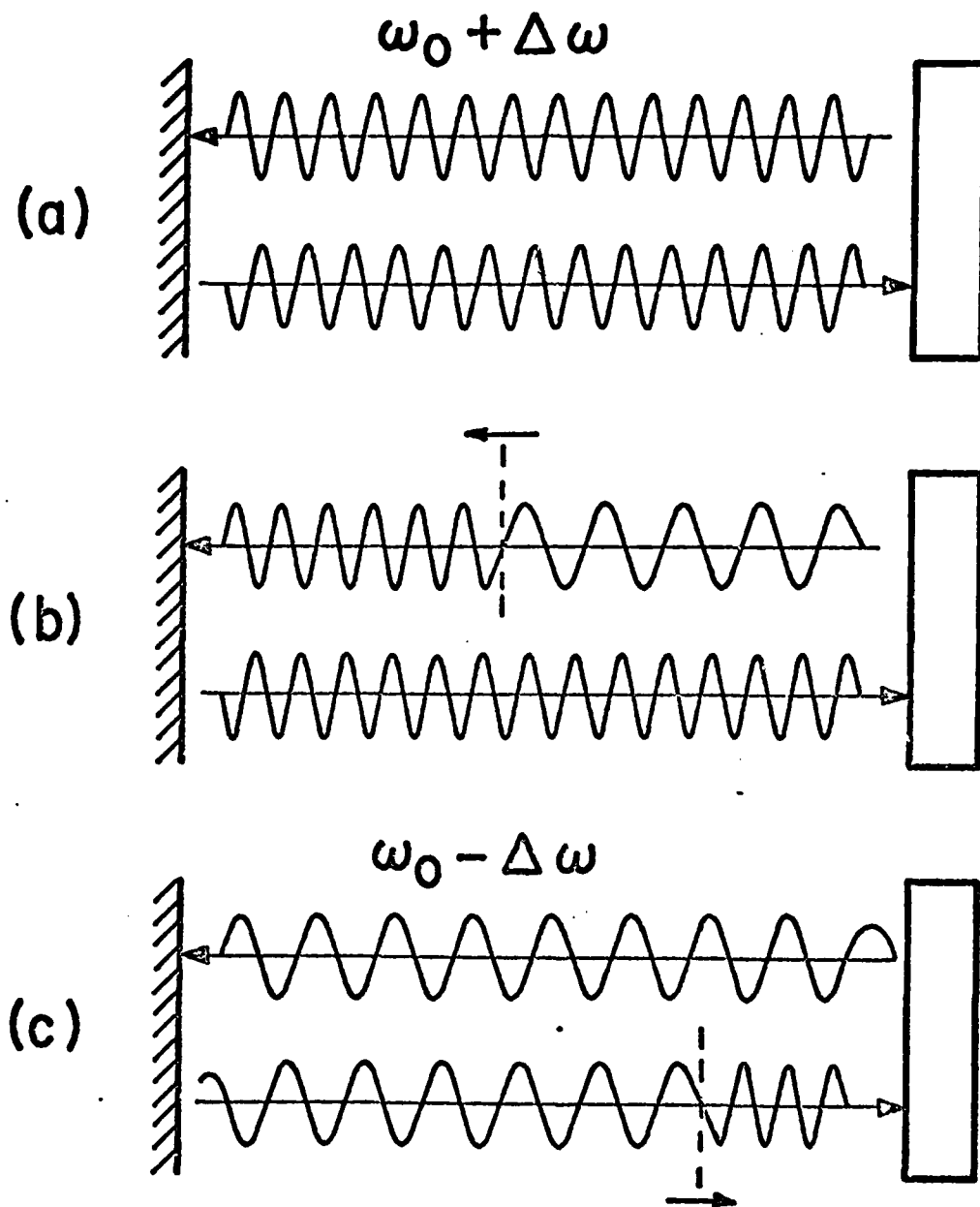


FIGURE 9